NASA TECHNICAL NOTE

NASA TN D-3287

NASA TN D-3287

AN ESTIMATE OF THE CHEMICAL KINETICS BEHIND NORMAL SHOCK WAVES IN MIXTURES OF CARBON DIOXIDE AND NITROGEN FOR CONDITIONS TYPICAL OF MARS ENTRY

by Robert L. McKenzie

Ames Research Center
Moffett Field, Calif.

NATIONAL AERONAUTICS AND SPACE ADMINISTRATION • WASHINGTON, D. C. • FEBRUARY 1966

AN ESTIMATE OF THE CHEMICAL KINETICS BEHIND NORMAL SHOCK WAVES IN MIXTURES OF CARBON DIOXIDE AND NITROGEN FOR CONDITIONS TYPICAL OF MARS ENTRY

By Robert L. McKenzie

Ames Research Center
Moffett Field, Calif.

NATIONAL AERONAUTICS AND SPACE ADMINISTRATION

For sale by the Clearinghouse for Federal Scientific and Technical Information
Springfield, Virginia 22151 – Price $3.00

AN ESTIMATE OF THE CHEMICAL KINETICS BEHIND NORMAL SHOCK WAVES IN MIXTURES OF CARBON DIOXIDE AND NITROGEN FOR CONDITIONS TYPICAL OF MARS ENTRY

By Robert L. McKenzie
Ames Research Center

SUMMARY

The chemical kinetics behind normal shock waves in mixtures of carbon dioxide and nitrogen are studied. Particular emphasis is placed on a shock speed of 8 km/sec in ambient gas compositions containing 5, 10, and 50 percent CO_2 by volume. These conditions are typical of those anticipated for entry into the Martian atmosphere. Ambient density is varied from 10^{-6} to 10^{-1} times that of the earth sea-level density. The species considered are CO_2, N_2, CO, NO, CN, O_2, C, O, and N. A system of 17 reactions is initially assumed and later reduced to 9 by removing those found insignificant to the gross thermochemical behavior. The methods used for estimating exchange reaction rates are discussed in detail, and a scheme for correlating experimental activation energies is suggested. General features of the nonequilibrium chemistry are presented followed by an analysis of the uncertainties due to possible errors in estimated reaction rates. Particular consideration is given to the kinetics of CN for shock speeds of 4 to 8 km/sec. The CN concentration is shown to rapidly overshoot its equilibrium value for most ambient densities and shock velocities anticipated during entry into the Martian atmosphere.

INTRODUCTION

Recent studies of high-speed entry into postulated Martian atmospheres (e.g., ref. 1) have indicated the need for an improved understanding of the chemical kinetics in shock heated mixtures of carbon dioxide and nitrogen. Numerous investigations have dealt with high temperature nonequilibrium phenomena in air and its constituents (e.g., refs. 2 and 3), but relatively few have concerned other gases. Howe and Sheaffer (ref. 4) estimated the chemical kinetics behind normal shock waves in pure CO_2, and Bortner (ref. 5) considered mixtures of CO_2 and N_2 but made only a cursory estimate of the reaction system.

This study is intended to provide a more inclusive estimate of the expected thermochemical behavior behind strong shock waves in mixtures of CO_2 and N_2 based on the experimental reaction-rate data available to date. The objective must be limited, however, to establishing only the qualitative nature of the post-shock chemical kinetics since current experimental reaction-rate data are sparse and many theoretical rate estimates are incorporated. In light of the limited experimental data, it is also unjustified to retain any consideration of physical phenomena which have less that a major effect on the results. Regardless of these unavoidable inaccuracies, the qualitative

characteristics of these results may still be shown to be unique. This is accomplished by estimating reasonable limits to the errors in the theoretical reaction rates and applying them to obtain extreme kinetic profiles. The resulting profiles are then compared for all cases.

The controlling kinetic mechanism of the chemical system is estimated by considering all reactions among a prescribed set of species which are thought to have possible significance to the gross thermochemical behavior. Those reactions and species which then prove to be of secondary importance are eliminated and the small effects of their absence demonstrated.

The flow-field model chosen is that behind a normal shock wave because of its simplicity and direct application to most shock-tube experiments. The principal quantities defining the shock-wave conditions are shock speed, ambient gas composition, and ambient density. Ambient temperature, whose value is incidental to the results, was fixed at 200° K.[1] A single shock speed of 8 km/sec was selected for detailed study but lower speeds to 4 km/sec are also discussed. The speed of 8 km/sec was chosen principally because it represents a typical Mars entry condition and also because it serves to define the predominant chemical mechanisms for the lower speeds considered. The ambient densities considered are 10^{-6} to 10^{-1} times the earth sea-level density. These values bracket the high-speed flight regime of aerodynamic interest during any planetary entry. The ambient gas compositions selected are 5, 10, and 50 percent CO_2 (by volume) with the remainder, N_2. They were chosen in view of the three Mars atmosphere models given by reference 6.

It is emphasized that the results given by this study are to be considered preliminary estimates only. They may be assumed as qualitatively correct, but are subject to substantial quantitative adjustment as additional experimental results become available.

SYMBOLS

$\bar{A}$	frequency factor, defined by equation (8), m^3/mole-sec
D	molecular bond or dissociation energy, J
E_a	endothermic activation energy, J
F	partition function per unit volume
f_t, f_r, f_v	partition functions for translation, rotation, and vibration, respectively
H_R	endothermic heat of reaction, J

[1]Ambient temperature affects only the temperature ratio across a strong shock wave but has negligible effects on the absolute values of any quantity behind the wave front.

h	Planck's constant, 6.6256×10^{-34} J sec
K_c	equilibrium constant based on molar concentrations
k	Boltzmann constant, 1.3805×10^{-23} J/°K
k_f, k_b	reaction rate coefficient in the forward (endothermic) and reverse directions, respectively
l	total number of significant rotational degrees of freedom
M	an arbitrary chemical species acting as a collision partner
m	molecular mass, kg/particle
$\hat{m}$	molecular weight, kg/kg-mole
$\bar{m}$	$\hat{m}_2/\hat{m}_1$, also equal to the ratio: moles of ambient gas mixture per mole of local gas mixture
N_A	Avogadro's number, 6.022×10^{23} particles/mole
N_j	mole fraction, moles of species j per mole of local mixture
n	number of atoms per molecule
Q_{ij}	volumetric rate of production of species j by reaction i, moles/sec m^3
$\bar{Q}_{ij}$	species production rate parameter, $Q_{ij}\left(\frac{\hat{m}_1 y_o}{\rho_1 V_s}\right)\left(\frac{\rho_o}{\rho_1}\right)$
S_∞	collision cross section (see eq. (4))
s	total number of vibrational degrees of freedom
T	temperature, °K
T_1	ambient temperature, 200° K
$\bar{T}$	$\frac{T_2}{T_1}$
t	particle time, sec
t_L	laboratory time, sec
V	volume
V_s	shock speed, m/sec
v	local speed behind the shock wave (shock wave reference frame)

$\bar{v}$	$\frac{v}{V_s}$
y	distance behind the shock front, m
y_o	reference distance, 1 m
$\bar{y}$	distance parameter, $\frac{\rho_1}{\rho_o}\frac{y}{y_o}$
α	an index representing a vibrational energy mode
β,η	constants in equation (3)
γ_j	local concentration of species j, moles of j per mole of ambient gas
θ_r	characteristic temperature for rotation, ^oK
θ_{v_α}	characteristic temperature of the α vibrational mode, ^oK
$\bar{\mu}$	reduced molecular weight, $\frac{\hat{m}_A\hat{m}_B}{\hat{m}_A+\hat{m}_B}$
ρ	mass density, kg/m^3
ρ_o	reference density, 1.225 kg/m^3 (standard earth sea level)
$\bar{\rho}$	$\frac{\rho_2}{\rho_1}$
σ	symmetry number in equation (2)
[A]	concentration of species A in moles per unit volume

Subscripts

A,B,AB	evaluated for the particle A, B, or AB
e,(e)	equilibrium value
f	frozen chemistry value
i	reaction i
j	species j
(p)	peak concentration
r	reactant r

o reference value

1 conditions of the gas mixture ahead of the shock wave

2 conditions of the gas mixture behind the shock wave

METHOD OF ANALYSIS

General Considerations and Assumptions

This analysis is based on the following assumptions: A normal shock wave propagates at constant velocity into a quiescent mixture of CO_2 and N_2 of uniform density and temperature. After passage of the shock front the molecular internal energy modes of rotation, vibration, and electron excitation reach equilibrium with the translational energy prior to the onset of any chemical change. The mixture of chemical species mixture just behind the shock, which is the same as that ahead, then starts from its so-called "frozen chemistry" condition and proceeds through a system of homogenous bimolecular reactions to an equilibrium state. All the molecular energy modes follow in equilibrium with the local translational temperature. It is well known that some of these assumptions, although classical, are not always valid, particularly that of locally equilibrated vibrational energies. In view of the qualitative nature of this study, however, the addition of any further refinements is unjustified.

Chemical species.- The complexity of the chemical system to be analyzed depends primarily on the number of species considered. The species important to the chemical kinetics are assumed in this case to be those significant in determining the equilibrium thermodynamic state of the gas. From reference 7, these are shown for shock speeds of 4 to 8 km/sec to be: CO_2, N_2, CO, NO, CN, O_2, C, O, and N. Assuming only these species simplifies this study since, at the high temperatures associated with "frozen chemistry" immediately behind the shock, the gas tends toward complete ionization. The consequences of this assumption should not be serious, however, since at the shock speeds of interest, the ionization rates are comparable to the chemical rates in an environment moving toward negligible ionization (e.g., ref. 8). Furthermore, the estimates of reference 5 which included ionization reactions and shock speeds up to 12 km/sec indicate that even for much higher speeds than 8 km/sec, the nonequilibrium concentration of ionized species is not predominant compared to the concentration of neutral species. Thus, the consideration of ionized species is not expected to significantly affect the conclusions of this study. References 9, 10, and 11 provide the relative abundances of ionized and uncharged particles for the frozen and equilibrium thermodynamic states of present interest.

Consistent with the assumption of a locally equilibrated distribution of internal energies, specific consideration of the species in internally excited states is also omitted. Excited species have been shown to react at higher rates than their ground-state counterparts but the effects of such considerations can be assumed absorbed into the given mean reaction rates which account for reactants in all energy states. This is the case when rate coefficients

are determined from experiment since most analyses of such experiments assume an equilibrium distribution of energy states except when specific excitation reaction rates are given.

Reactions.- The preliminary set of reactions used for this study is given by table I. Each reaction is written with the endothermic direction from left to right. The reactions are divided into three general groups, according to the manner in which they were studied. The dissociation reactions (No. 1-6) are considered fundamental to the reaction system and were included in all calculations of the chemical kinetics. In this study they are assumed to occur upon collision of the dissociating species with any arbitrary particle, M. This assumption is a convenient means of simplifying the reaction system although using an arbitrary collision partner rather than a specific one can in some cases lead to a factor of 20 error in reaction rate. Because there are many other uncertainties which must be incorporated that preclude the penalties of this one, the benefits of a simplified system make the assumption attractive. The air exchange reactions (No. 7-9) are those familiar to most nonequilibrium air studies. Their rates have been measured many times and they are considered to contribute comparatively little uncertainty to the results of this analysis. The remaining reactions (No. 10-17) are those resulting from the presence of carbon atoms and molecules containing them. The eight carbon reactions given represent less than half the combinations possible from the species considered. The others fall into several groups, all of which have been omitted. For example, six more reactions may be written which contain the same reactants as given in table I but result in different products. A typical example is shown with reaction 14, given below with its endothermic heat of reaction.

$$CO + NO \leftrightarrows CO_2 + N \qquad 102 \text{ kJ/mole}$$

The heat of reaction provides an indication of the energy required to activate the reaction. These same reactants could also yield

$$CO + NO \leftrightarrows CN + O_2 \qquad 424 \text{ kJ/mole}$$

What appear to be simpler and more likely products in this reaction require a much higher energy to occur. The corresponding increase in activation energy affects the associated reaction rate in an exponential manner making the reaction far less effective than its lower energy counterpart. Hence, the higher energy versions of a given set of reactants are omitted. Another group of possible reactions not included in table I are those resulting in three products. The same reactants used above could also yield the following:

$$CO + NO \leftrightarrows CN + 2O \qquad 917 \text{ kJ/mole}$$

It is easily seen that the same arguments applied above may again be used in this case. Additional energy is required to produce the third product thereby allowing three-product exchange reactions to be ignored as possible controlling reactions.

A third group of reactions which bear discussion are those containing species of primary interest but also requiring a species which is not significant

in determining the post-shock equilibrium state of the gas. An example is given by

$$2CN \rightleftarrows N_2 + C_2 \qquad 29 \text{ kJ/mole}$$

Even though this reaction requires relatively little energy, it necessitates admitting to the presence of C_2. Since C_2 always appears in extremely small quantities under the circumstances of interest here, the CN lost or generated by this mechanism is trivial compared to other higher energy reactions using more predominate species. Thus, reactions involving such species as C_2, N_2O, and NO_2, to name a few, may be neglected and their kinetics studied using the thermodynamic profiles computed in their absence. In view of the preceding arguments, table I is believed to contain all the reactions of primary importance to the chemical system for the shock-wave conditions of this study. It also contains a few which may be superfluous because of the nature of the system. These are identified in the "Results and Discussion" section by comparing the relative effectiveness of all the reactions in producing a given species.

Reaction Rates

Before proceeding to an application of the postulated chemical system, it is first necessary to define the rate coefficients associated with each reaction. A review of recent literature (e.g., ref. 2) has shown that for air reactions of interest, a given rate is seldom known within a factor of 5 at high temperatures. Fortunately, there are some exceptions such as N_2 and O_2 dissociation rates which have been claimed accurate within a factor of 2 when collision partners are specified. However, in the cases where limited or no measured data are available, it can be considered exceptional to predict the correct rates within an order of magnitude. This "plus or minus one order-of-magnitude" criteria will be used to evaluate the theoretical predictions made in this study. The reactions given in table I may be separated for this purpose into two types, dissociation and exchange. Because of this separability, it is advantageous to use the rate theory found most successful for each type.

Dissociation reactions.- Because the dissociation reactions are assumed in this study to occur only with a general collision partner, it is necessary to use a rate theory that will aid in unifying the many published rates which specify collision partners. Also, a method is required to predict the rate of CN dissociation, the only dissociation reaction where no data were found. A recent and successful theory formulated by Hansen (ref. 12) from a version of the available energy theory is used for these purposes. Hansen's results may be applied to the general dissociation reaction

$$AB + M \underset{k_f}{\overset{k_b}{\leftrightarrows}} A + B + M \qquad (1)$$

The rate of production of molecule A, for example, by the above mechanism is defined as

$$\frac{d[A]}{dt} = \frac{2k_f}{\sigma}[M]\left\{[AB] - \frac{1}{K_c}[A][B]\right\} \tag{2}$$

where it is assumed that $K_c = k_f/k_b$

$$\sigma = \begin{cases} 1, & A \equiv B \\ 2, & A \not\equiv B \end{cases} \qquad \text{and} \qquad k_f = k_f(T)$$

The forward rate coefficient, k_f, can be equated to that given by Hansen. Rather than use Hansen's results directly, however, two slight modifications were made to his expression for k_f which allows it to be compared with the convenient Arrhenius form

$$k_f = \beta T^{\eta} \exp(-E_a/kT) \tag{3}$$

This is accomplished by neglecting the change in momentum cross section with increasing particle momentum and assuming $D/kT \gg 1/2$. A difference of less than 5 percent is introduced in the final results at the temperatures of interest here. The modified Hansen equation for collision induced dissociation of a diatomic molecule, AB where $AB \not\equiv M$, is then given by

$$k_f = \left(\frac{8kN_A}{\pi\bar{\mu}}\right)^{1/2} \frac{4S_\infty}{3\sqrt{\pi e}} \left(\frac{D}{k}\right)^{3/2} T^{-1} \exp\left(-\frac{D}{kT}\right) \tag{4}$$

where e is the Napierian base. In equation (4), S_∞ is equivalent to the Sutherland cross section used for viscosity (values given for several species in ref. 12) and D is the bond dissociation energy of molecule AB. Rewriting equation (4) using the mean values, $S_\infty = 30\times10^{-20}m^2$ and $\bar{\mu} = 14$, appropriate for diatomic molecules containing C, N, and/or O, we have

$$k_f = 2\times10^{6} \left(\frac{D}{k}\right)^{3/2} T^{-1} \exp\left(-\frac{D}{kT}\right) \frac{m^3}{\text{mole-sec}} \tag{5}$$

(It should be noted that the values of k_f given in this paper are 10^{-6} times those given in the more customary units of cm^3/mole-sec.) Equation (5) is compared with several published rate equations for O_2, N_2, NO, and CO dissociation in figure 1. The published rates are plotted without giving consideration to their applicable temperature ranges although the composite experimental temperature limits of the individual experiments are indicated. Equation (5) is shown to provide rates which represent an approximate mean of the other values plotted; it therefore seems appropriate to use equation (5) for predicting the unknown CN dissociation rates. The difficulty in choosing among rate coefficients where collision partners are specified is also avoided by using equation (5) to define k_f for all the dissociation reactions in table I except reaction 1 (CO_2 dissociation).

Hansen (ref. 12) also derives a dissociation rate theory for polyatomic molecules such as CO_2. When the results are compared with experimental data, however, they are not found to be so successful as for the diatomic case. Furthermore, several recent measurements of CO_2 dissociation rates given in references 14 to 17 are shown by figure 2 to be in good agreement. Figure 2 also includes Hansen's unadjusted prediction which is shown to be high. The experimental results of Davies (refs. 16 and 17) were selected and have been used here as the CO_2 dissociation rate for reaction 1.

Exchange reactions.- Of the eleven exchange reactions listed in table I only reactions 7 to 9 have rate coefficients based on experiment. Their values, taken from references 2 and 3, are given in table I. The remaining rates for the carbon reactions must be estimated. A review of the literature resulted in finding several methods for making such estimates but none showed substantial improvement over the classical quantum mechanical approximation described in reference 18. The method, commonly termed "Absolute Reaction Rate Theory" or "Transition-State Theory," is also discussed with greater detail in the more recent references 19 and 20. The transition-state theory has an advantage over some other methods such as "collision theory" (see ref. 19) in that it contains greater molecular detail. In view of the structural similarity of the carbon, nitrogen and oxygen atoms which make up this kinetic system, the transition-state theory also lends itself to a convenient generalization based on a system for classifying the reactions, as will now be shown. The theory may be applied in one form to bimolecular reactions such as that given in general terms by

$$AB + CD \rightarrow \left(\begin{matrix} AB \\ CD \end{matrix}\right)_* \rightarrow AC + BC \tag{6}$$

where A, B, C, and D may be atoms or molecules. The asterisk refers to the unstable "activated complex" which serves as a transition molecule during the reaction. The forward reaction-rate coefficient, k_f, is similar in definition to that used in equation (2) and is expressed by the transition-state theory as

$$k_f = \frac{kT}{h} \frac{F_*}{\prod_r F_r} \exp\left(-\frac{E_a}{kT}\right) \tag{7}$$

In equation (7), F_r is the partition function per unit volume of each reactant, r, and F_* is the same as F_r but for the activated complex less the contribution of one vibrational mode. The omitted vibration is the mechanism by which the complex is assumed to separate into reaction products. The transition-state theory does not provide a means of estimating the activation energy, E_a. Such estimates will be discussed subsequently; here we are dealing only with the pre-exponential or "frequency factor" defined as

$$\bar{A} \equiv \frac{kT}{h} \frac{F_*}{\prod_r F_r} \tag{8}$$

The partition functions, F_r and F_*, are evaluated assuming equipartition of energies and contributions of molecular translation, rotation, and vibration only. Thus

$$F = \frac{f_t f_r f_v}{V} \tag{9}$$

where

$$f_t = \left(\frac{2\pi mkT}{h^2}\right)^{3/2} V \tag{10a}$$

$$f_r = \left(\frac{T}{\theta_r}\right)^{1/2} \tag{10b}$$

$$f_v = \prod_{\alpha=1}^{s} \left(1 - e^{-\theta_{v_\alpha}/T}\right)^{-1} \tag{10c}$$

At this point, one could substitute values of the individual molecular properties and evaluate $\bar{A}$ for each reaction in detail. However, this is not practical since these properties, which are well known for most reactants, are difficult to determine for an activated complex. Furthermore, equation (7) is derived by assuming a physical model of the reaction process which is highly idealized and also requires E_a to be estimated. It therefore appears equally reliable to express $\bar{A}$ in a general sense for a given set of similar reactions (i.e., with similar reactants). The approach here will be to demonstrate the similarity of the C, O, and N atoms and through this similarity construct a set of reaction-rate approximations based on the molecular configuration of pairs of reactants. To this end, table II lists values of $\hat{m}$, θ_r, and θ_v required by equations (10) for the species of interest. It can be seen that when properly grouped like quantities show a degree of similarity. For example, the monatomic species are of nearly the same atomic weight and, from the periodic table, have similar atomic structures. In the case of the diatomic species an average value of θ_r or θ_v can be found which adequately approximates the thermodynamic properties of any of them. The same is true for the polyatomic molecules when the molecular arrangement is considered (i.e., linear or nonlinear). The individuality of each species can therefore be dropped and attention given only to the number of atoms in each molecule and the manner in which they are arranged. This technique has been proposed in several references (e.g., ref. 21) but with different results since the constants chosen were for more arbitrary reactants. The results given here are specialized for C, O, and N systems.

Generalized rate coefficients.- Consider the general bimolecular reaction given by equation (6). If equation (9) is substituted into equation (8) and the contribution from each reactant is denoted by an appropriate subscript

$$\bar{A}_{\text{eq.}(6)} = \frac{kT}{h} \frac{V(f_t f_r f_v)_*}{(f_t f_r f_v)_{AB}(f_t f_r f_v)_{CD}} \tag{11}$$

If now AB is an atom (called B) and CD a diatomic molecule, the reaction is

$$B + CD \rightarrow \left(\begin{matrix} B \\ CD \end{matrix}\right)_* \rightarrow \text{products} \tag{12}$$

Since $f_{r_B} = f_{v_B} = 1$, equation (11) becomes

$$\bar{A}_{\text{eq.}(12)} = \frac{kT}{h} \frac{V(f_t f_r f_v)_*}{f_{t_B}(f_t f_r f_v)_{CD}} \tag{13}$$

Thus, $\bar{A}$ takes a special form for reactants of the molecular configuration in equation (12). This scheme of reaction classification is now extended to other reactant configurations using suitable average values of the molecular constants.

The translational energy contributions are treated first since all particles contain a translational energy mode. The translational terms, therefore, may be factored from equation (11) for any reaction. Incorporating equation (10a) equation (11) is then rewritten as

$$\bar{A} = C\bar{\mu}^{-3/2} T^{-1/2} \frac{(f_r f_v)_*}{(f_r f_v)_{AB}(f_r f_v)_{CD}} \tag{14a}$$

where the constant

$$C = \frac{k}{h}\left(\frac{2\pi k}{h^2}\right)^{-3/2}$$

($C = 6.68 \times 10^7$ for $\bar{A}$ in m^3/mole-sec) and $\bar{\mu}$ is a reduced molecular weight. If an average molecular weight of 14 is used for all atomic particles, $\bar{\mu}$ is approximated by

$$\bar{\mu} = 14 \frac{n_{AB} n_{CD}}{n_{AB} + n_{CD}} \tag{14b}$$

The rotational partition functions are approximated using equation (10b) with average values of θ_r. From table II the average values selected are

$$\text{Diatomic molecules} \quad \theta_r \approx 3.3^\circ \text{ K}$$

$$\text{Polyatomic molecules} \quad \theta_r \approx 0.6^\circ \text{ K}$$

When the proper values of l are substituted into equation (10b)

$$f_r \approx \begin{cases} 1 & \text{Atoms} & l = 0 \\ 0.3T & \text{Diatomic and linear molecules} & l = 2 \\ 2T^{3/2} & \text{Nonlinear molecules} & l = 3 \end{cases} \tag{15}$$

If θ_{V_α}/T is assumed small, the vibrational contributions as represented by equation (10c) can be approximated by

$$f_V \approx \prod_{\alpha=1}^{s} \frac{T}{\theta_{V_\alpha}} \tag{16}$$

The values of θ_{V_α} given by table II are replaced by average values selected as

$$\theta_{V_1} = 2900^\circ \text{ K} \qquad \theta_{V_4} = 4300^\circ \text{ K } (930^\circ \text{ K for linear molecules})$$

$$\theta_{V_2} = 1900^\circ \text{ K} \qquad \theta_{V_5} = 4300^\circ \text{ K}$$

$$\theta_{V_3} = 930^\circ \text{ K} \qquad \theta_{V_\alpha} = 5000^\circ \text{ K for } \alpha > 5$$

The number of vibrational degrees of freedom, s, must still be determined. The value assigned to a particular molecule depends on the number of atoms, n, in the molecule. Since an activated complex has one less vibrational mode than its molecular counterpart, the following rules apply:

$$s = \begin{cases} 3n-5 & \text{Linear or diatomic molecules} \\ 3n-6 & \text{Linear complex or nonlinear molecule} \\ 3n-7 & \text{Nonlinear complex} \end{cases}$$

All activated complexes are assumed nonlinear and the vibrational mode corresponding to θ_{V_1} is considered the mode causing destruction of the complex. From the preceding, f_V is then given for the configurations needed as

$$f_V = \begin{cases} 3.4\times10^{-4}T & \text{Diatomic molecule} \\ 5.7\times10^{-7}T^2 & \text{Triatomic complex} \\ 2.0\times10^{-10}T^3 & \text{Nonlinear triatomic molecule} \\ 2.1\times10^{-13}T^4 & \text{Linear triatomic molecule} \\ 6.1\times10^{-18}T^5 & \text{Four atom complex} \\ 4.9\times10^{-29}T^8 & \text{Five atom complex} \end{cases} \tag{17}$$

The combined results of equations (14) to (17) are then as follows: Denoting an atom as A, a diatomic molecule as A·B or C·D, a linear triatomic molecule as C·D·E, and a nonlinear triatomic molecule as $D^C E$, we have

Reactant pair	$\bar{A}$(m^3/mole-sec)
A+B·C	$2\times10^{4}T$
A+C·D·E	$3\times10^{2}T$
A+D^{C}E	$5\times10^{-2}T^{3/2}$
A·B+C·D	$1\times10^{-3}T^{2}$
A·B+C·D·E	$2\times10^{-5}T^{2}$
A·B+D^{C}E	$3\times10^{-9}T^{5/2}$

(18)

These are the values of $\bar{A}$ used for reactions 10 to 17 in table I.

Comparisons with experiment.- Figure 3 provides comparisons of equation (18) with values of $\bar{A}$ obtained by experiment or other estimates. The applicability of figure 3 relies on the assumption that the Arrhenius form of k_f (eq. (3)) is valid over any temperature range. It is generally accepted that this is not the case but since all of the experimental results plotted in figure 3 were obtained by fitting equation (3) to the basic data, figure 3 should at least provide an indication of the theoretical accuracy. The figures are therefore intended as a comparison of the predicted magnitudes of $\bar{A}$ with experiment in the experimental temperature range ($\log T \approx 3$) and also as a comparison of the functional dependence of $\bar{A}$ on temperature as given by theory with that indicated by experiment (i.e., by comparing the slopes of the lines plotted). The experimental values plotted are extrapolated considerably beyond the temperature limits of their associated experiment. The maximum temperature of most experiments represented did not exceed 5000° K. The three general reactions shown are those used for this study. The shaded box on each figure indicates the range of nonequilibrium temperatures covered for V_s = 8 km/sec and the assumed inaccuracy of $\bar{A}$. The specific comparative rates are from the references given in parentheses beside the reaction. Figure 3 relies on the premise that a method successful in predicting N, O reactions works equally well for C, N, O reactions because of the similarity of the carbon atom to the nitrogen and oxygen atoms. This premise is necessary since only N, O reaction rates were available for comparison. Figures 3(a) and 3(b) show excellent agreement between theory and experiment considering the gross assumptions made. A probable error factor of plus or minus an order of magnitude is assigned for further analysis of the reaction-rate uncertainties. This error factor is based on the experimental results shown although larger errors may exist. In figure 3(c) the scatter in experimental values does not allow any definite conclusions regarding the accuracy of the theory. The experimental values for a single reaction are not in good agreement (viz., $N_2+O_2 \rightarrow 2NO$). An error factor of plus or minus two orders of magnitude is therefore assigned to reactions of this type. Fortunately, such reactions involving two diatomic reactants can be shown to be minor contributors to this kinetic system unless their rates exceed the present estimates by four or five orders of magnitude. It is seen from figure 3(c) that this is conceivable but it is believed unlikely.

Activation energy.- An estimation of k_f using equation (7) still requires a value of the activation energy, E_a. A method of estimating E_a using intermolecular potential energy surfaces is described in reference 18 but it requires elaborate computing techniques which are not warranted considering the approximate nature of this study. Some semiempirical rules have also been proposed by Glasstone, Laidler, and Eyring (ref. 18) and Hirchfelder (ref. 22) but were adjusted for reactions involving hydrogen and do not give good results for the N, O reactions. An empirical scheme was therefore constructed which follows the basic ideas of reference 18 but is centered on N, O reactions (assuming again that C, N, O, and N, O reactions are similar). This scheme results in an empirical relation which is general for all types of bimolecular reactions used here and is written for an endothermic process.

To facilitate a discussion of types of reactions, the following endothermic reaction types are identified:

I	$AB+M \rightarrow A+B+M$	dissociation
II	$AB+C \rightarrow A+BC$	three center exchange
III	$AB+CD \rightarrow AC+BD$	four center exchange

where each symbol is an atom or pair of atoms not separated by the reaction. The following postulates are proposed:

(1) For Type I reactions, $E_a = H_R = D_{AB}$. The validity of this has been demonstrated experimentally with a few exceptions such as CO_2 dissociation. It is also reflected in equation (4) for dissociation reaction-rate coefficients.

(2) For any reaction occurring directly from ground-state reactants, $E_a \geq H_R$. Measurement verifies this for all of the exchange reactions examined, and it is a requirement from an energy conservation viewpoint.

(3) E_a is a function of the sum of the bond dissociation energies for those bonds which are broken in the reaction. This presumption is a result of the methods suggested in references 18 and 22. It may be given a pseudophysical basis by relating it to the energy required to destroy the activated complex and neglecting its heat of formation.

Regardless of the lack of rigor in the preceding postulates, they appear to represent the behavior of experimental observations and are therefore pursued. Normalizing with respect to H_R, the third postulate gives

$$\frac{E_a}{H_R} = f\left(\frac{\Sigma D_r}{H_R}\right) \tag{19}$$

The boundary conditions become $E_a/H_R = 1$ when $(\Sigma D_r)/H_R = 1$ and $E_a/H_R \geq 1$ always. Equation (19) suggests a correlation of experimental results as given by figure 4. The data are taken from reference 2 and pertain to N, O reactions except where noted otherwise on the figure. A linear correlation is obtained

on semilog axes if the likely degree of error in the experimental data is kept in mind and temperature dependencies are ignored. From figure 4, the following empirical relation is then proposed:

$$\frac{E_a}{H_R} = \exp\left\{\frac{1}{10}\left(\frac{\Sigma D_r}{H_R} - 1\right)\right\} \tag{20}$$

The error assigned to the results of figure 4 requires a multiplying factor for the right-hand side of equation (20) of exp ± 3/10. For values of $H_R/k < 50{,}000^\circ$ K, this error affects k_f by less than an order of magnitude (H_R/k is less than $50{,}000^\circ$ K for most of the carbon exchange reactions and all those of importance). Equation (20) was used to complete the estimates of k_f for reactions 10 to 17 of table I.

Computing Method

The nonequilibrium properties behind a normal shock wave were computed using a modified version of the IBM 704 program described by references 23 and 24. The system of equations will not be discussed in detail here because of the completeness in description supplied by reference 24. However, in brief, the program relies on conventional gasdynamic and chemical conservation equations in conjunction with a quantum-mechanical description of the individual species thermodynamics. Thus, spectroscopic data such as that given in table II are used as input. Some additional input data also required were the heats of formation of the individual species and were obtained from reference 25. The computer program given by reference 24 was recoded for use on an IBM 7094 and modified to accept polyatomic molecules with up to nine vibrational degrees of freedom. Equilibrium electron excitation has also been included as in the original program. Electronic energy levels up to 80,000 cm^{-1} (1.6×10^{-18} J) were incorporated although such refinement has only small effects on the numerical results of this study.

Computing time was found to have a much stronger dependence on the number of species than on the number of reactions. Minor species retained in the calculations slow the computing progress appreciably and, in some cases, their computed concentrations suffer from excessive numerical errors. Typical computing times for a relaxation to within 10 percent of equilibrium at V_s = 8 km/sec were about 5 minutes.

RESULTS AND DISCUSSION

With all the necessary reactions and rate coefficients established, this section is devoted to an analysis of the chemical kinetics for shock conditions described previously. A discussion is first given of some results using the nominal reaction rates in table I. General characteristics of the chemical kinetics are illustrated and several features which are independent of the reaction-rate errors are discussed. This is followed by an evaluation of the changes in thermochemical profiles due to uncertainties in the reaction rates. The consequences of deleting certain species and reactions from the chemical system are also investigated in an effort to simplify the kinetic model.

Finally a brief study is made of the CN kinetics over a range of shock speeds because of the particular interest in that species for studies of shock-layer radiation.

General Characteristics

Some estimates of the nonequilibrium chemical behavior for a shock speed of 8 km/sec using nominal reaction rates are presented in figures 5 to 7. Thermodynamic profiles and species concentrations are plotted as functions of the distance parameter $\bar{y}$, which is equivalent to a binary scaling parameter as described by reference 26. The parameter $\bar{y}$ may be converted to laboratory time by the approximation

$$t_L \approx \frac{\bar{y} y_o}{(\rho_1/\rho_o) V_s} \tag{21}$$

which is correct within 10 percent for all shock conditions considered. Part (a) of each figure illustrates profiles of the thermodynamic quantities most sensitive to the chemical kinetics. Other thermodynamic variables which are not shown, such as local pressure or enthalpy, vary only a few percent behind the shock wave. Local velocity is also omitted since, for a normal shock wave, it is easily obtained from

$$\bar{v} = \frac{1}{\bar{\rho}} \tag{22}$$

Part (b) of each figure illustrates the individual species concentrations given as mole fractions of the ambient gas mixture. These may be converted to the more familiar mole fractions based on local gas composition by

$$N_j = \bar{m} \gamma_j \tag{23}$$

The equilibrium thermodynamic and species concentration values given in figures 5 to 7 were obtained using a computer program developed by Simcox and Peterson (ref. 9). The equilibrium species concentration levels indicated separately on the figures are for $\rho_1/\rho_o = 10^{-6}$ only since the nonequilibrium curves for $\rho_1/\rho_o = 10^{-1}$ achieve equilibrium levels within the scale of the figures. In some cases, slight differences between the fundamental inputs used in reference 9 and in this study preclude a close comparison of equilibrium species concentrations with the nonequilibrium profiles. However, the discrepancy never exceeds 5 percent. Tabulated equilibrium concentration values are given in table III to provide those numerically too low to appear on the figures.

Figures 5 to 7 demonstrate several features of the chemical kinetics which are retained regardless of the reaction rates used. For example, the profiles, when plotted in terms of $\bar{y}$, show no dependence on ambient density until equilibrium is nearly achieved. This occurs because the dissociation reactions proceed predominantly in the forward direction (except near equilibrium) while the exchange reactions are binary in either direction. Among other

things, this correlation allows easy estimation of the time or distance to equilibrium for intermediate ambient densities. That is, if the equilibrium values of any quantity sensitive to the kinetics are known, the manner in which its values depart from the lowest density curve to approach equilibrium is not difficult to estimate. (Equilibrium thermodynamic properties and species concentrations for initial gas mixtures close to those used here are given by ref. 11.) A second feature demonstrated in figures 5 to 7 pertains to the manner in which those species quickly generated (e.g., NO and CN) tend to overshoot their equilibrium concentrations. A "peak" concentration for each generated species may be defined whether it is actually achieved or not. It depends only on the shock speed and ambient gas composition, assuming reaction rates are known. This density-independent peak is achieved if the equilibrium concentration is less than the peak value. In the event that the equilibrium concentration is greater, the concentration will rise monotonically. An example of both cases can be found in figure 6(b) by comparing the CN concentrations for $\rho_1/\rho_o = 10^{-6}$ and 10^{-1}. Notice in the case where $\rho_1/\rho_o = 10^{-6}$, the CN concentration reaches a peak and then decreases to its equilibrium value. This same behavior would occur for all lower densities and any higher density where the equilibrium CN concentration was less than the "peak." For those ambient densities where the equilibrium CN concentration was higher than the "peak," the CN concentration profile would rise monotonically as it does for $\rho_1/\rho_o = 10^{-1}$ shown in figure 6(b). By virtue of this same behavior, certain minor species which are strong radiant emitters (e.g., C_2) were also found to achieve concentrations considerably higher than their equilibrium value within the nonequilibrium region.

A comparison of the (a) parts of figures 5 to 7 to obtain the effects of ambient gas mixtures showed only minor differences for the mixtures considered. The differences in thermodynamic profiles arise principally because of small changes in their end points (i.e., the initial or frozen and equilibrium values). The time or distance required to reach near-equilibrium is essentially unaltered. Conversely, comparing part (b) of each figure shows ambient gas composition to have sizable effects on the species concentration but, again, the major differences are in the relative initial and equilibrium values rather than time or distance. However, the example is cited where decreasing the ambient gas composition from 50 to 5 percent CO_2 causes approximately a fourfold increase in $\bar{y}$ at the CN peak. On the other hand, $\bar{y}$ at the NO peak is unaffected.

To gain insight into the relative importance of each reaction to the whole chemical system it is worthwhile to compare the rate of production of certain species by individual reactions. Figure 8 makes these comparisons at one set of shock-wave conditions for all except the monatomic species. The dependent parameter, $\bar{Q}_{ij}$, in figure 8 is proportional to the species production rate defined by equation (2); that is, $\bar{Q}_{ij}$ in figure 8(a) represents the net production (or reduction) of CO by each reaction shown and accounts for both the forward and reverse contribution of that reaction. Some reactions (viz., 8 and 13, table I) show a negligible contribution to any total species production. Reaction 13 would not become significant unless k_f for that reaction was several orders of magnitude greater than those values regarded as reasonable (i.e., using the limits defined by fig. 3(c)). Reaction 8 has a relatively well-established rate which keeps it ineffective for any species production,

thus making it clearly unimportant (e.g., figs. 8(b) and 8(f)). Some other reactions appearing in figure 8 also show the possibility of being deleted. For example, reaction 16 (figs. 8(a) and 8(e)) is minor compared to other reactions contributing to the same species. Also, it is a reaction most probably already contained in the measured CO_2 dissociation rate (reaction 1) since it incorporates only products of CO_2. Its effect on the kinetics has been numerically tested and found to be negligible. Reactions 15 and 17 (figs. 8(a) and 8(f)) also incorporate only CO_2 and its products. However, they serve as principal O_2 generators and cannot be deleted when considering that species.

Figure 8 is representative of similar plots for other ambient densities and gas mixtures. The results of figure 8 are altered by higher ambient densities in a manner compatible with that of figures 5 to 7; that is, $\bar{Q}_{ij}$ for a higher density departs from the low density curves towards zero when equilibrium is approached. A change in gas mixture will cause some slight relative shifting of the $\bar{Q}_{ij}$ curves but does not alter the conclusions obtained regarding the importance of individual reactions. Hence, reactions 8, 13, and 16 may be deleted for all ambient densities, gas mixtures, and, in addition, other shock speeds.

Additional thermodynamic and species concentration profiles for $V_s = 6$ and 4 km/sec are presented in figures 9 and 10, respectively. These figures illustrate the diminishing differences between the frozen and equilibrium values of any quantity with decreasing shock velocity and show a lessening tendency of the generated species to reach high peak concentrations. The extent to which the nonequilibrium region is lengthened with decreasing shock velocity is also demonstrated. The effects of other ambient densities and gas compositions at these shock speeds are similar to those at $V_s = 8$ km/sec.

The Effects of Reaction-Rate Uncertainties

When the estimated errors which may be present in rate coefficients for the carbon exchange reactions are recalled (figs. 3 and 4), it is of interest to investigate their effects on the chemical behavior as given in figures 5 to 7. For this purpose, the shock conditions of figure 7 were chosen as an example since they are the most sensitive to reaction-rate uncertainties of all the cases shown. From the limits given by figures 3 and 4, rate combinations were chosen which would maximize or minimize the generated diatomic species concentrations since their behavior is the most sensitive to exchange reactions. To obtain a "maximum profile," maximum values were used for the rate coefficients of all reactions in question except 10. Figure 8(c) shows reaction 10 quickly reverses, thus it must be a minimum for maximum CN formation. The "minimum profiles" came from opposite considerations.

The resulting thermodynamic profiles, given by figure 11(a), are relatively insensitive to the rates used. In particular, local density is the variable most insensitive making its measurement inadequate for resolving chemical detail in a complicated system such as this one (density is commonly measured by interferometer or electron beam techniques to obtain rate information). In contrast to the thermodynamic quantities, figures 11(b) and 11(c)

show species concentrations to exhibit high sensitivity to the rate variations. This is particularly evident where the time or distance to a peak concentration and its associated magnitude are examined. Thus, in the absence of an ability to resolve chemical detail by other methods, considerable information may be gained by spectroscopically measuring the time to peak CN concentration for example. This technique would not provide individual reaction rates nor define the underlying mechanisms in the customary detail but it would allow a more refined reaction system model to be established, suitable for the needs of many predictions in aerodynamic applications.

Contributions of the O_2 Reactions

The analysis of experimental data for a chemical system of many species and reactions is always made simpler by removing as many insignificant variables as possible from the theoretical model. When only the gross thermochemical behavior is of interest, removal of any species or reaction reduces the number of reaction rates which must be measured and aids in reducing the numerical difficulties encountered when calculating such behavior.

The significance of the contributions of O_2 reactions to the remaining kinetic system becomes questionable when the results in figure 8 are examined. As seen there, none of the O_2 reactions are important to the formation of any species except O_2. Thus, the five reactions containing O_2 were deleted and the results compared to nonequilibrium profiles including them. Figure 12 gives one example of such a comparison. The case shown (50 percent CO_2) is that displaying the greatest effect of all the ambient mixtures considered using nominal reaction rates. The thermodynamic properties (fig. 12(a)) are shown to have a negligible dependence on O_2 while the effect on concentrations of other species is small (fig. 12(b)). These small effects are not enlarged when other reaction rates are used except in the extreme case where the O_2 reaction rates are maximized and the others put to a minimum. However, that situation is not seriously considered since experimental evidence favors the opposite case.[2] It is interesting to note that Howe and Sheaffer (ref. 4) also found the inclusion of O_2 unnecessary when considering 100 percent CO_2.

The effect of deleting the O_2 reactions in a 50 percent CO_2 mixture was also investigated at $V_s = 4$ km/sec where O_2 appears in larger equilibrium concentrations. The effects at that speed are larger but, again, they appear primarily in the species concentrations. Thus, for shock speeds greater than 4 km/sec and reaction rates equal to or greater than those used here, O_2 may be omitted without serious error. The results of such a deletion are a 20- to 40-percent reduction in computing time and a simplification of the reaction system from 14 to 9 reactions, assuming reactions 8, 13, and 16 have already been removed.

[2]"Experimental evidence" refers to some unpublished preliminary measurements of CN radiation intensities made by James Arnold of the Ames Research Center. The data were taken behind incident shock waves in a shock tube at conditions close to those considered here and indicated a relatively rapid formation of CN.

Cyanogen Kinetics

Special attention is given here to the kinetics of CN because of its importance to the total radiant emission from behind shock waves in these gas mixtures. Figure 13 gives an estimate of the CN concentration at its peak value and the laboratory time to reach the peak for a range of shock speeds and two gas mixtures. The nominal reaction rates were used for this calculation and the 5 percent CO_2 mixture was omitted because of its close proximity to the 10 percent CO_2 case. The possible error in this estimate may be evaluated by considering the variations in definition of the CN peak as shown in figure 11(b). The percentage of shifting due to reaction-rate uncertainties shown in figure 11(b) at $V_s = 8$ km/sec is essentially preserved at the lower speeds. The effect of ambient gas composition on CN peak concentration can be seen from figure 13 to be fairly significant. Figure 14 compares the peak (as given in fig. 13) with the equilibrium CN concentrations for the densities used in this study. It is of interest to note (cf., figs. 14(a) and 14(b)) that for a given shock speed the 50 percent CO_2 mixture has a greater tendency to achieve a peak CN concentration than the 10 percent CO_2 mixture; that is, the magnitudes of the peak concentrations lie above the equilibrium concentrations for a greater range of ambient densities in the 50 percent CO_2 case. Thus, nonequilibrium CN radiation, for example, at a given ambient density and shock speed, may be more significant for the higher initial CO_2 concentration mixtures at least up to 50 percent CO_2 and particularly at shock speeds less than 8 km/sec. This may be compared to conclusions drawn from equilibrium results (see, e.g., ref. 7) which show maximum CN equilibrium concentrations to occur when the initial CO_2 content is 9 to 16 percent.

Finally, attention is called to the trends shown in figure 14(b) at $V_s < 5$ km/sec. The extreme overshoot of the CN concentration at these lower speeds is typical in regions where the amount of CN present is most sensitive to temperature. It can be seen from the equilibrium curves that small increases in V_s (or correspondingly, in temperature), in the region of $V_s = 5$ km/sec, produces large increases in equilibrium concentration. Thus there is, in effect, a "cutoff temperature" below which the CN concentrations are negligible. If, as in the case for $V_s < 5$ km/sec, the equilibrium temperature is less than the cutoff temperature but the nonequilibrium temperatures are greater, there will be extreme overshooting of the CN concentration in the nonequilibrium region. However, it should also be noted that although the ratio of peak to equilibrium concentrations is large at these conditions, the magnitude of the peak concentration is still much lower than those achieved at higher shock speeds. Thus, the effects of nonequilibrium phenomena on CN radiation intensities (for example) may be more pronounced at shock speeds less than 5 km/sec and at a given density but the magnitude of the intensity will also be very low. Similar behavior at higher shock speeds is found for other minor species such as C_2, N_2O, and NO_2.

CONCLUDING REMARKS

A study of the chemical kinetics behind normal shock waves in mixtures of CO_2 and N_2 has been made as a prelude to experimental investigations. Emphasis

was placed on shock conditions typical of those anticipated during entry into the Martian atmosphere. A shock speed of 8 km/sec was studied in detail but lower speeds are also discussed. Ambient gas mixtures containing 5, 10, and 50 percent CO_2 and ambient densities of 10^{-6} and 10^{-1} times that of sea level were considered.

A survey of current methods of estimating reaction rates became necessary. It was found that most of the dissociation reaction rates could be based on measured data and that an adequate theory was available for estimating those that could not. Most of the exchange reactions required estimated rates and the "transition-state" approximation was used. The results were compared with measured data where available, and agreement was found to be satisfactory. A scheme for correlating activation energies and predicting unknown values was also devised for reactions containing C, N, and O atoms.

The species considered were CO_2, N_2, CO, NO, CN, O_2, C, O, and N. An original system of 17 bimolecular reactions was reduced to 14 for the species above. Deletion of O_2 and its reactions introduced only small errors and further reduced the chemical system to 9 reactions. They are

$$CO_2 + M \leftrightarrows CO + O + M$$

$$N_2 + M \leftrightarrows 2N + M$$

$$NO + M \leftrightarrows N + O + M$$

$$CO + M \leftrightarrows C + O + M$$

$$CN + M \leftrightarrows C + N + M$$

$$N_2 + O \leftrightarrows NO + N$$

$$N_2 + C \leftrightarrows CN + N$$

$$CO + N \leftrightarrows CN + O$$

$$CO + NO \leftrightarrows CO_2 + N$$

The remaining O_2 reactions, important mainly to the production of O_2 itself are

$$O_2 + M \leftrightarrows 2O + M$$

$$NO + O \leftrightarrows O_2 + N$$

$$CO_2 + O \leftrightarrows CO + O_2$$

$$CO + O \leftrightarrows O_2 + C$$

The chemical kinetics were found to allow the assumptions of binary scaling over most of the nonequilibrium region. This led to a correlation of the dependence on ambient density and allowed density-independent results to be presented except near equilibrium.

Certain generated species such as CO, NO, CN, and O_2 were shown to overshoot their equilibrium concentrations for most ambient densities of interest in the flight regime. This was particularly the case for CN which suggests significant nonequilibrium radiant emission at low densities.

The effects of ambient gas composition on the length or duration of the nonequilibrium region behind the shock wave were shown to be small. The principal differences in thermochemical profiles between the several ambient gas compositions are due to changes in relative magnitudes of the profile end points rather than the time or distance required to reach near-equilibrium.

Admitting errors of plus or minus an order of magnitude in the estimated reaction rates caused only small differences in the predicted thermodynamic profiles. The species concentration profiles, however, are very sensitive to such error. Measurement of the time to peak concentration of an identifiable species was shown to be a possible means of establishing rate information.

Special attention was given to the kinetics of CN. It appears to be one of the species most sensitive to ambient gas composition and reaction-rate uncertainties. CN displayed a greater tendency to overshoot its equilibrium concentration in increasing ambient proportions of CO_2 to 50 percent CO_2.

At shock speeds less than 5 km/sec, the CN concentrations are small in the nonequilibrium region but still several orders of magnitude greater than their equilibrium value. The extent of concentration overshoot decreases with increasing shock velocity but remains significant at the shock speeds of interest for entry into the Martian atmosphere.

Ames Research Center
National Aeronautics and Space Administration
Moffett Field, Calif., Oct. 8, 1965

REFERENCES

1. Arnold, James O.; Reis, Victor H.; and Woodward, Henry T.: Theoretical and Experimental Studies of Equilibrium and Nonequilibrium Radiation to Bodies Entering Postulated Martian and Venusian Atmospheres at High Speeds. AIAA paper 65-116.

2. Bortner, M. H.: Chemical Kinetics in a Reentry Flow Field. R63SD63 Space Sciences Lab., General Electric Missile and Space Div., Aug. 1963.

3. Wray, Kurt L.: Chemical Kinetics of High Temperature Air. International Hypersonics Conference, M.I.T., Cambridge, Aug. 16-18, 1961, (Progress in Astronautics and Rocketry, vol. 7, Hypersonic Flow Research) Academic Press, 1962, pp. 181-204.

4. Howe, John T.; and Sheaffer, Yvonne S.: Chemical Relaxation Behind Strong Normal Shock Waves in Carbon Dioxide Including Interdependent Dissociation and Ionization Processes. NASA TN D-2131, 1964.

5. Bortner, M. H.: Chemical Kinetics of Planetary Entry. Symposium on Dynamics of Manned Lifting Planetary Entry, Philadelphia, 1962, S. M. Scala, A. C. Harrison, and M. Rogers, eds., John Wiley and Sons, Inc., 1963, pp. 172-184.

6. Levin, George M.; Evans, Dallas E.; and Stevens, Victor, eds.: NASA Engineering Models of the Mars Atmosphere for Entry Vehicle Design. NASA TN D-2525, 1964.

7. Woodward, Henry T.: Thermodynamic Properties of Carbon-Dioxide and Nitrogen Mixtures Behind a Normal Shock Wave. NASA TN D-1553, 1963.

8. Eschenroeder, A. Q.; Daiber, J. W.; Golian, T. C.; and Hertzberg, A.: Shock Tunnel Studies of High-Enthalpy Ionized Airflows. AGARD-NATO Specialists Meeting, Rhode-Saint-Genese, Belgium, 1962, The High Temperature Aspects of Hypersonic Flow (AGARDograph 68), 1964, pp. 217-184.

9. Simcox, Craig D.; and Peterson, Victor L.: Charts for Equilibrium and Frozen Flows Across Plane Shock Waves in Carbon Dioxide. NASA SP-3018, 1965.

10. Bailey, Harry E.: Equilibrium Thermodynamic Properties of Carbon Dioxide. NASA SP-3014, 1965.

11. Bailey, Harry E.: Equilibrium Thermodynamic Properties of Three Engineering Models of the Martian Atmosphere. NASA SP-3021, 1965.

12. Hansen, C. Frederick: Estimates for Collision-Induced Dissociation Rates. AIAA Jour., vol. 3, no. 1, Jan. 1965, pp. 61-66.

13. Davies, William O.: Radiative Energy Transfer on Entry Into Mars and Venus. IITRI-T200-8, Quart. Rep. 8. (NASA Contract NASr-65(01)), IIT Res. Inst., Aug. 1964.

14. Brabbs, Theodore A.; Belles, Frank E.; and Zlatarich, Steven A.: Shock-Tube Study of Carbon Dioxide Dissociation Rate. J. Chem. Phys., vol. 38, no. 8, April 15, 1963, pp. 1939-1944.

15. Steinberg, M.: Carbon Dioxide Dissociation Rates Behind Shock Waves. TR64-49, G.M. Defense Res. Lab., Sept. 1964.

16. Davies, William O.: Carbon Dioxide Dissociation at 3500° to 6000° K. J. Chem. Phys., vol. 41, no. 6, Sept. 15, 1964, pp. 1846-1852.

17. Davies, William O.: Radiative Energy Transfer on Entry Into Mars and Venus. IITRI-T200-7, Quart. Rep. 7. (NASA Contract NASr-65(01)), IIT Res. Inst., June 1964.

18. Glasstone, Samuel; Laidler, Keith J.; and Eyring, Henry: The Theory of Rate Processes. McGraw-Hill Book Co., Inc., 1941.

19. Benson, Sidney William: The Foundations of Chemical Kinetics. McGraw-Hill Book Co., Inc., 1960.

20. Clarke, John Frederick; and McChesney, M.: The Dynamics of Real Gases. Butterworths, Inc., 1964.

21. Nawrocki, Paul J.; and Papa, Robert: Atmospheric Processes. Prentice-Hall, Inc., 1963.

22. Hirschfelder, Joseph O.: Semi-Empirical Calculations of Activation Energies. J. Chem. Phys., vol. 9, no. 8, Aug. 1941, pp. 645-653.

23. Marrone, Paul V.: Inviscid, Nonequilibrium Flow Behind Bow and Normal Shock Waves, Part I. General Analysis and Numerical Examples. Cornell Aero. Lab., Inc., Rep. QM-1626-A-12(1), May 1963.

24. Garr, Leonard J.; and Marrone, Paul V.: Inviscid, Nonequilibrium Flows Behind Bow and Normal Shock Waves, Part II. The IBM 704 Computer Programs. Cornell Aero. Lab., Inc., Rep. QM-1626-A-12(II), May 1963.

25. McBride, Bonnie J.; Heimel, Sheldon; Ehlers, Janet G.; and Gordon, Sanford: Thermodynamic Properties to 6000° K for 210 Substances Involving the First 18 Elements. NASA SP-3001, 1963.

26. Gibson, W. E.; and Marrone, P. V.: Nonequilibrium Scaling Criterion for Inviscid Hypersonic Airflows. Cornell Aero. Lab., Inc., Rep. QM-1626-A-8, Nov. 1962.

TABLE I.- PRELIMINARY REACTION SYSTEM

No.	Group	Reaction	Assumed reaction-rate terms*	
			$\bar{A}$	$\frac{E_a}{k}$ (°K)
1	Dissociation	$CO_2+M \rightleftarrows CO+O+M$	$1.2\times10^{5}T^{1/2}$	34360
2	Dissociation	$N_2+M \rightleftarrows 2N+M$	$8.6\times10^{13}T^{-1}$	113350
3	Dissociation	$NO+M \rightleftarrows N+O+M$	$2.9\times10^{13}T^{-1}$	75560
4	Dissociation	$CO+M \rightleftarrows C+O+M$	$8.5\times10^{13}T^{-1}$	128960
5	Dissociation	$CN+M \rightleftarrows C+N+M$	$5.2\times10^{13}T^{-1}$	94140
6	Dissociation	$O_2+M \rightleftarrows 2O+M$	$2.6\times10^{13}T^{-1}$	59390
7	Air exchange	$NO+O \rightleftarrows O_2+N$	$3.2\times10^{3}T$	19680
8	Air exchange	$N_2+O_2 \rightleftarrows 2NO$	2.0×10^{8}	61600
9	Air exchange	$N_2+O \rightleftarrows NO+N$	7.0×10^{7}	38000
10	Carbon exchange	$N_2+C \rightleftarrows CN+N$	$2\times10^{4\mp1}T$	31560
11	Carbon exchange	$CO+N \rightleftarrows CN+O$	$2\times10^{4\mp1}T$	45800
12	Carbon exchange	$CO_2+N \rightleftarrows CN+O_2$	$3\times10^{2\mp1}T$	49560
13	Carbon exchange	$N_2+CO \rightleftarrows CN+NO$	$1\times10^{-3\mp2}T^{2}$	92010
14	Carbon exchange	$CO+NO \rightleftarrows CO_2+N$	$1\times10^{-3\mp2}T^{2}$	20980
15	Carbon exchange	$CO_2+O \rightleftarrows CO+O_2$	$3\times10^{2\mp1}T$	18210
16	Carbon exchange	$2CO \rightleftarrows CO_2+C$	$1\times10^{-3\mp2}T^{2}$	72390
17	Carbon exchange	$CO+O \rightleftarrows O_2+C$	$2\times10^{4\mp1}T$	69570

*$k_f = \bar{A} \exp\left(-\frac{E_a}{kT}\right) \frac{m^3}{mole\text{-}sec}$

TABLE II.- SOME MOLECULAR CONSTANTS

Species	$\hat{m}$	θ_r(°K)	θ_{v_α}(°K)			
			α=1	α=2	α=3	α=4
C	12.011					
O	16.000					
N	14.007					
CO	28.011	2.78	3122			
NO	30.007	2.45	2740			
CN	26.018	2.73	2976			
N_2	28.014	5.78	3395			
O_2	32.000	4.16	2274			
C_2	24.022	4.70	2362			
*CO_2	44.011	1.12	3380	1928	960	960
*N_2O	44.014	0.60	3199	1849	847	847
**NO_2	46.007	0.36	2332	1899	932	

*Linear molecule
**Nonlinear molecule

TABLE III.- EQUILIBRIUM SPECIES CONCENTRATIONS (γ_j) FOR V_s = 8 km/sec

Ambient mixture	5 percent CO_2 - 95 percent N_2		10 percent CO_2 - 90 percent N_2		50 percent CO_2 - 50 percent N_2	
$\frac{\rho_1}{\rho_0}$	10^{-6}	10^{-1}	10^{-6}	10^{-1}	10^{-6}	10^{-1}
C	4.41^{-2}	3.60^{-2}	7.87^{-2}	6.49^{-2}	2.35^{-1}	1.60^{-1}
O	9.13^{-2}	9.06^{-2}	1.77^{-1}	1.74^{-1}	7.35^{-1}	6.69^{-1}
N	1.35	9.46^{-1}	1.26	8.64^{-1}	7.99^{-1}	4.90^{-1}
CO	5.61^{-3}	4.75^{-3}	2.17^{-2}	1.96^{-2}	2.64^{-1}	3.03^{-1}
NO	9.67^{-5}	4.34^{-3}	1.67^{-4}	8.11^{-3}	3.50^{-4}	2.26^{-2}
CN	8.05^{-4}	9.78^{-3}	1.48^{-3}	1.84^{-2}	2.62^{-3}	3.69^{-2}
O_2	3.90^{-8}	1.94^{-5}	1.50^{-7}	7.74^{-5}	2.61^{-6}	1.28^{-3}
N_2	2.80^{-1}	4.79^{-1}	2.72^{-1}	4.64^{-1}	1.02^{-1}	2.32^{-1}
CO_2	2.12^{-9}	3.20^{-7}	1.03^{-8}	2.61^{-6}	2.67^{-7}	1.86^{-4}
$\bar{m}$	0.564	0.639	0.551	0.623	0.469	0.522

Note: A number such as 0.0025 appears as 2.5^{-3} in the table.

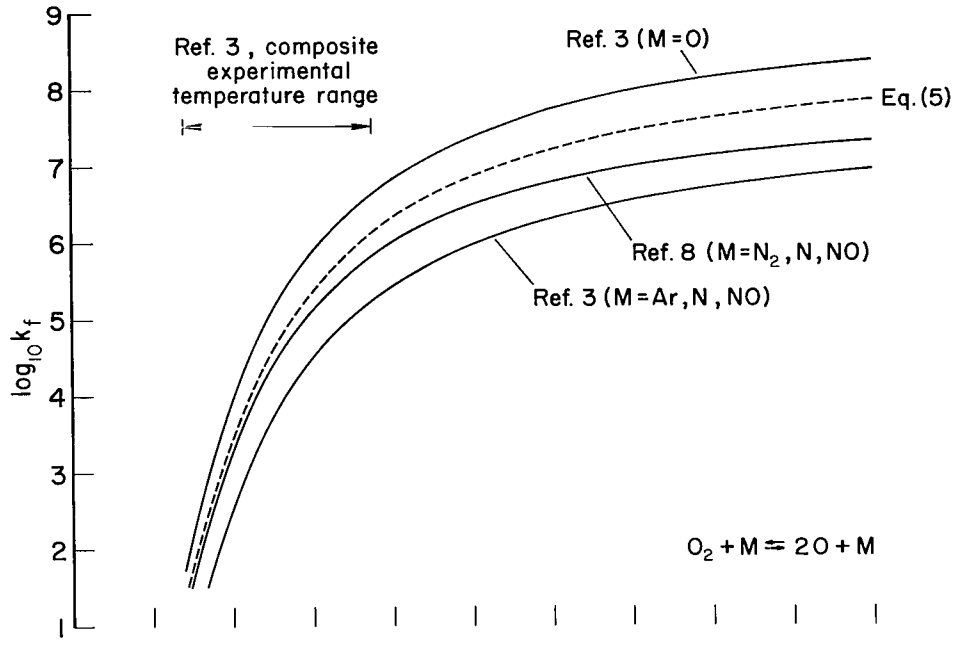

(a) O_2 dissociation.

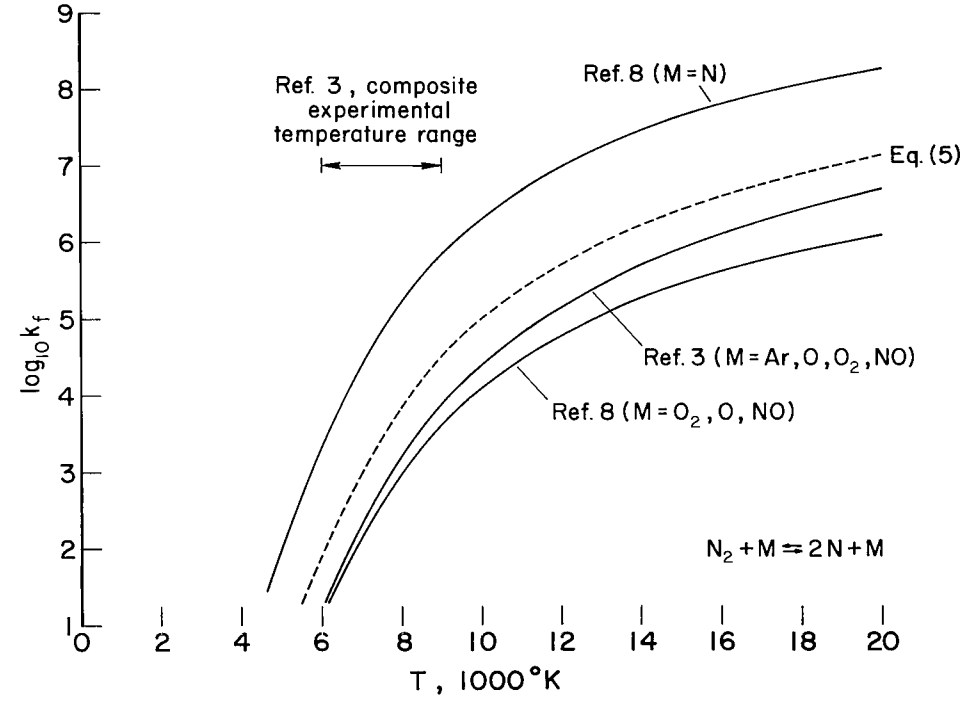

(b) N_2 dissociation.

Figure 1.- Comparison of dissociation reaction rate coefficients.

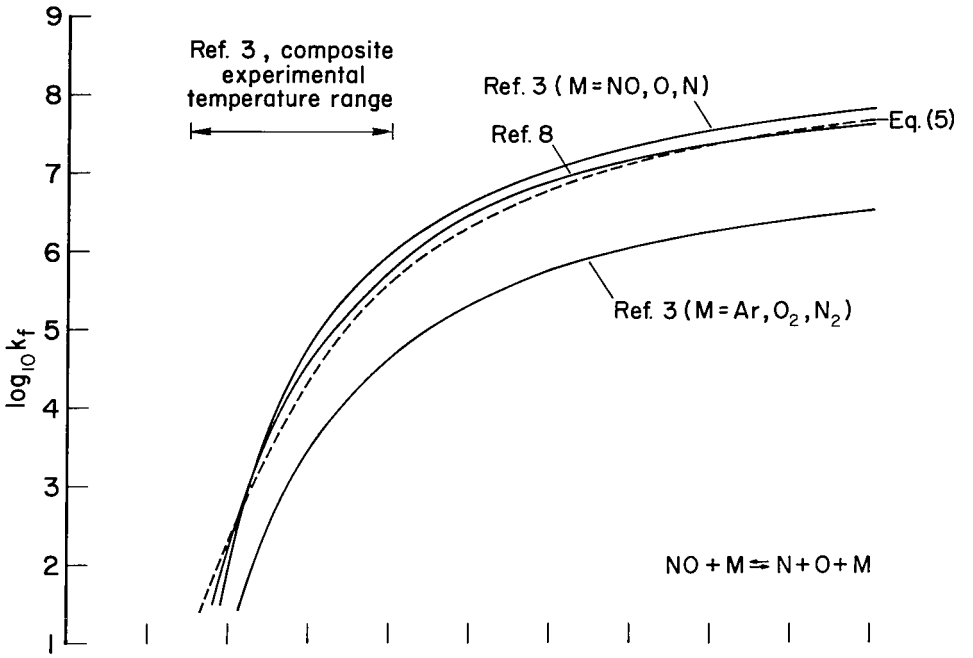

(c) NO dissociation.

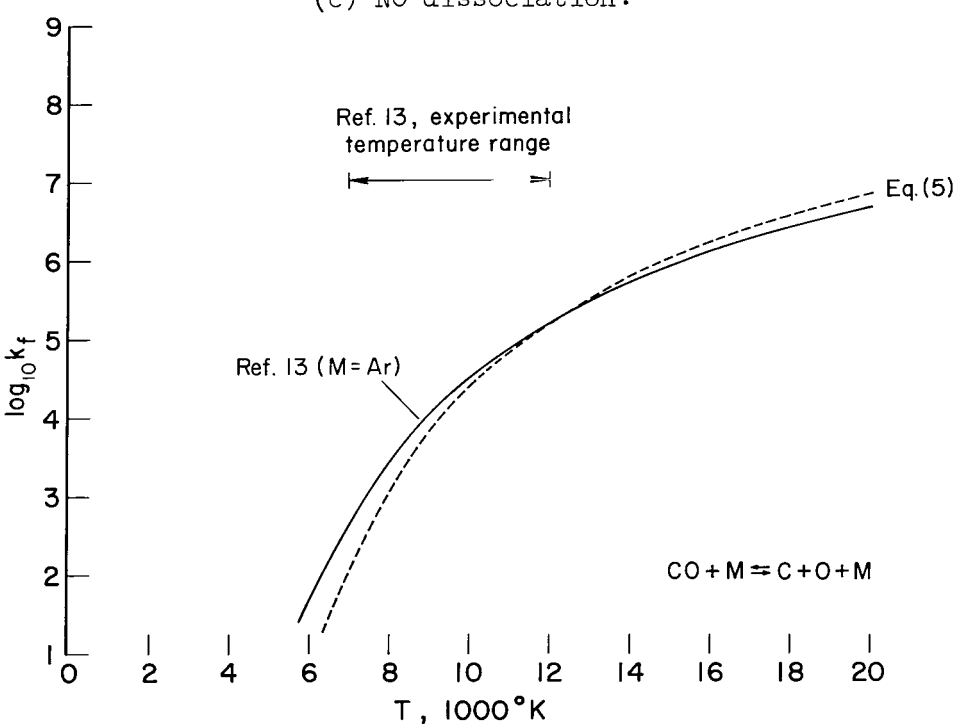

(d) CO dissociation.

Figure 1.- Concluded.

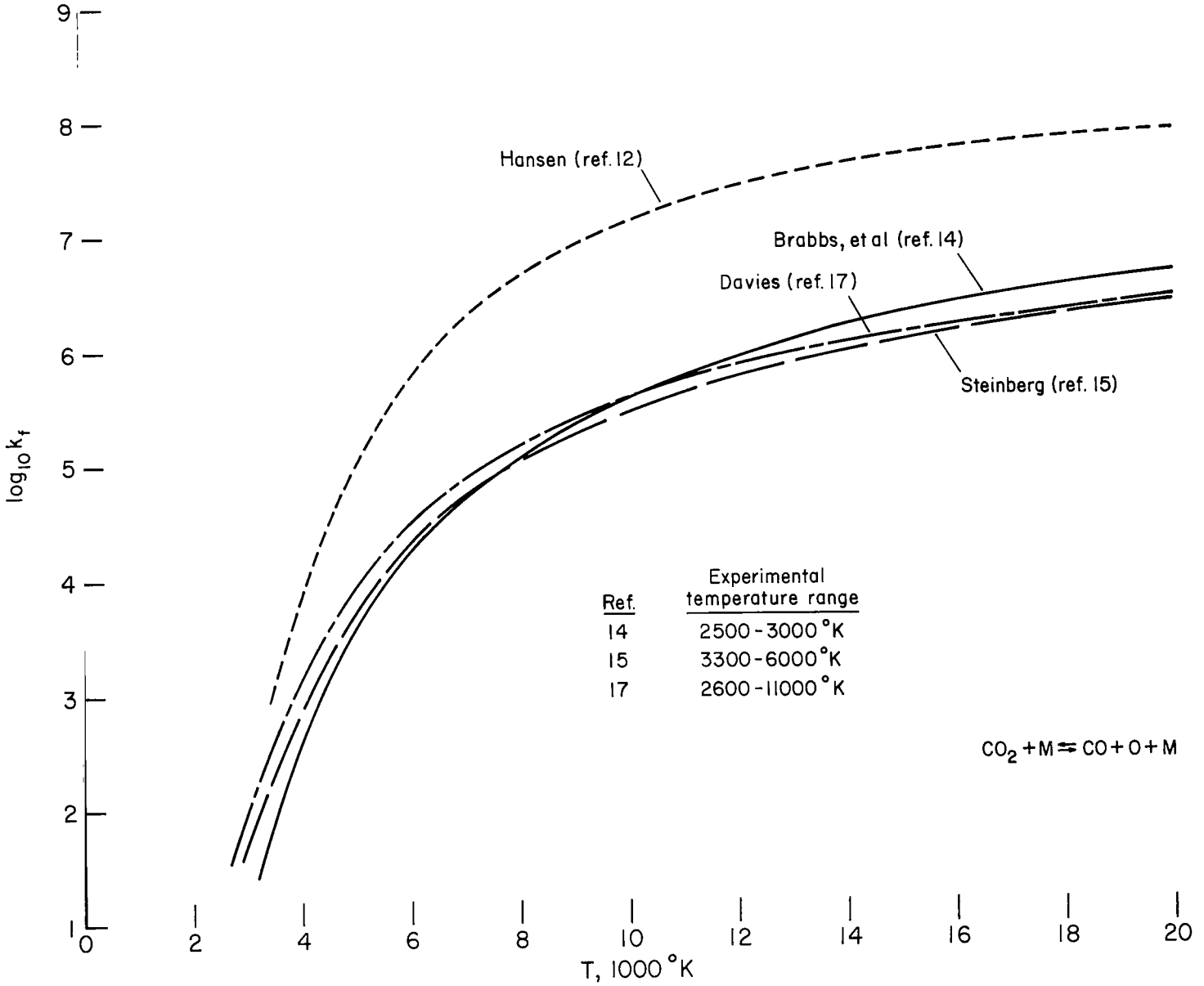

Figure 2.- CO_2 dissociation rate coefficients.

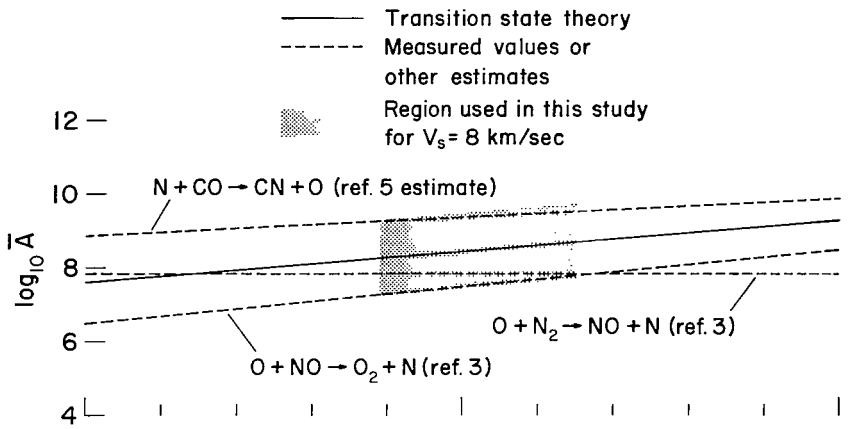

(a) Reactions of the type A+B·C → products.

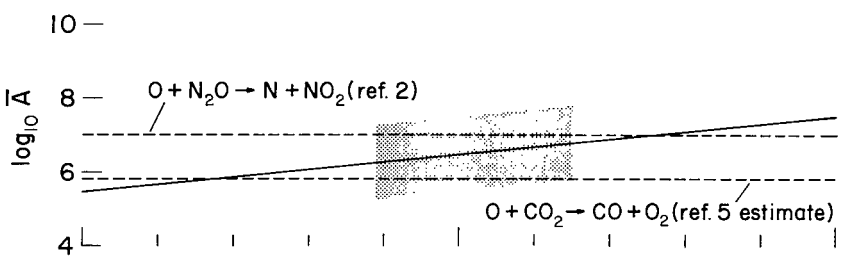

(b) Reactions of the type A+B·C·D → products.

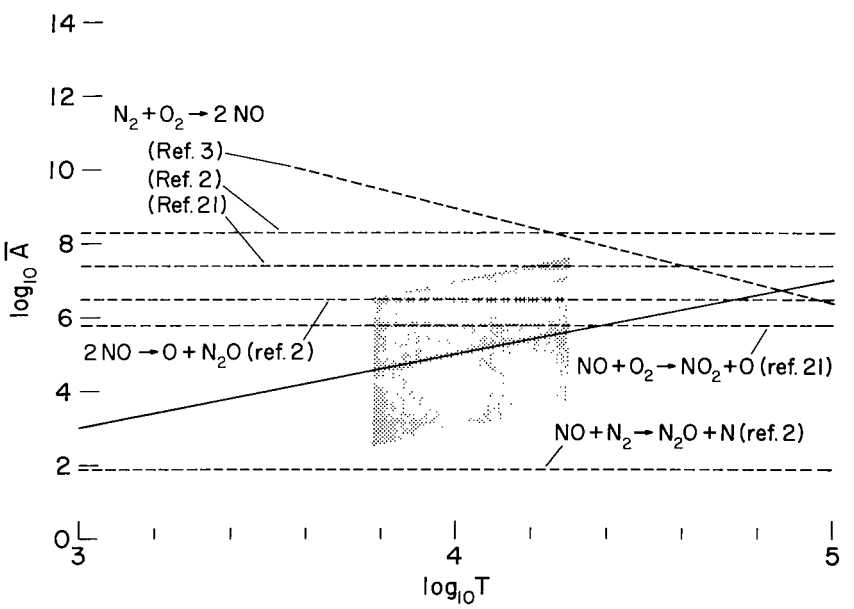

(c) Reactions of the type A·B+C·D → products.

Figure 3.- Frequency factors for some exchange reactions.

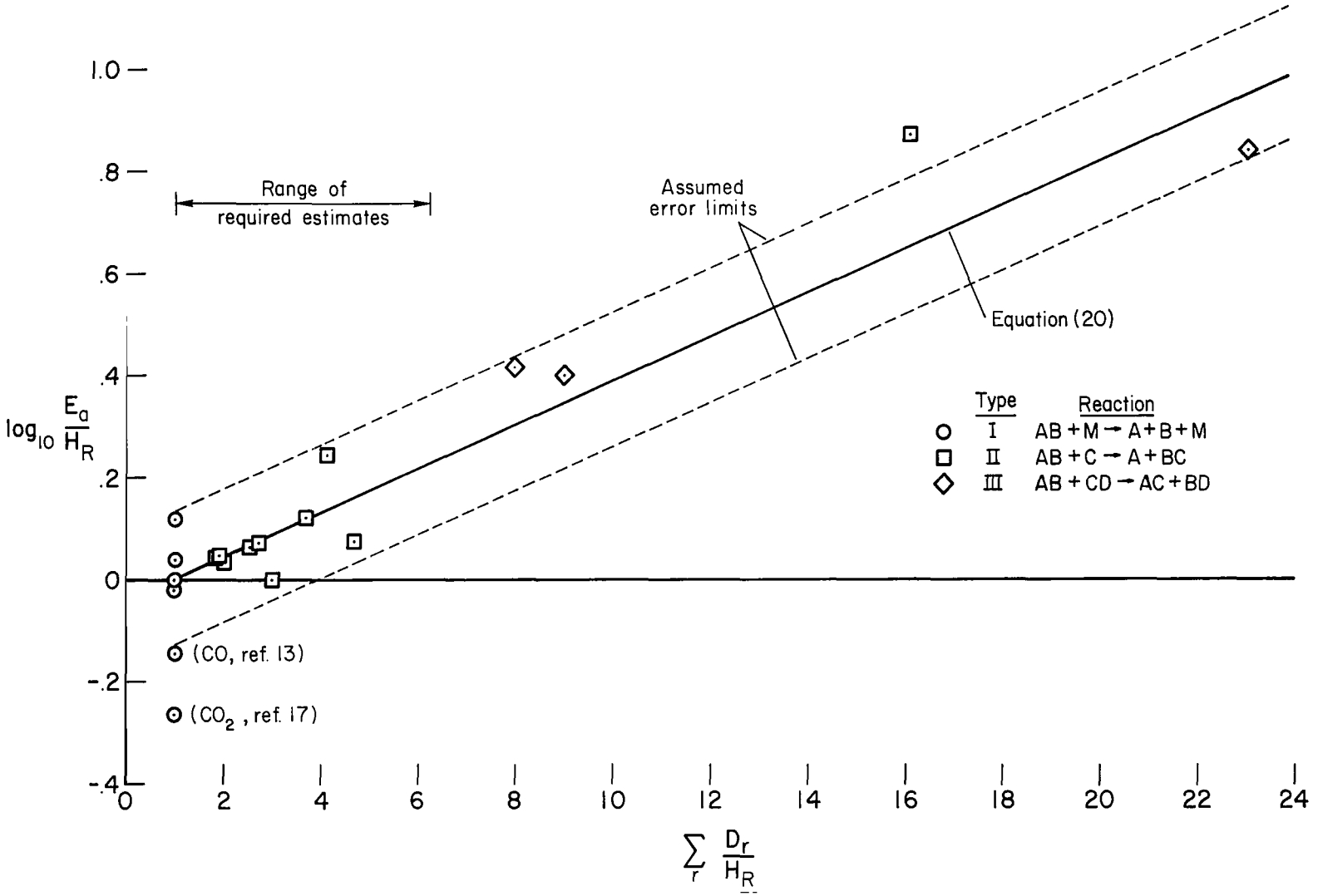

Figure 4.- Endothermic activation energy correlation.

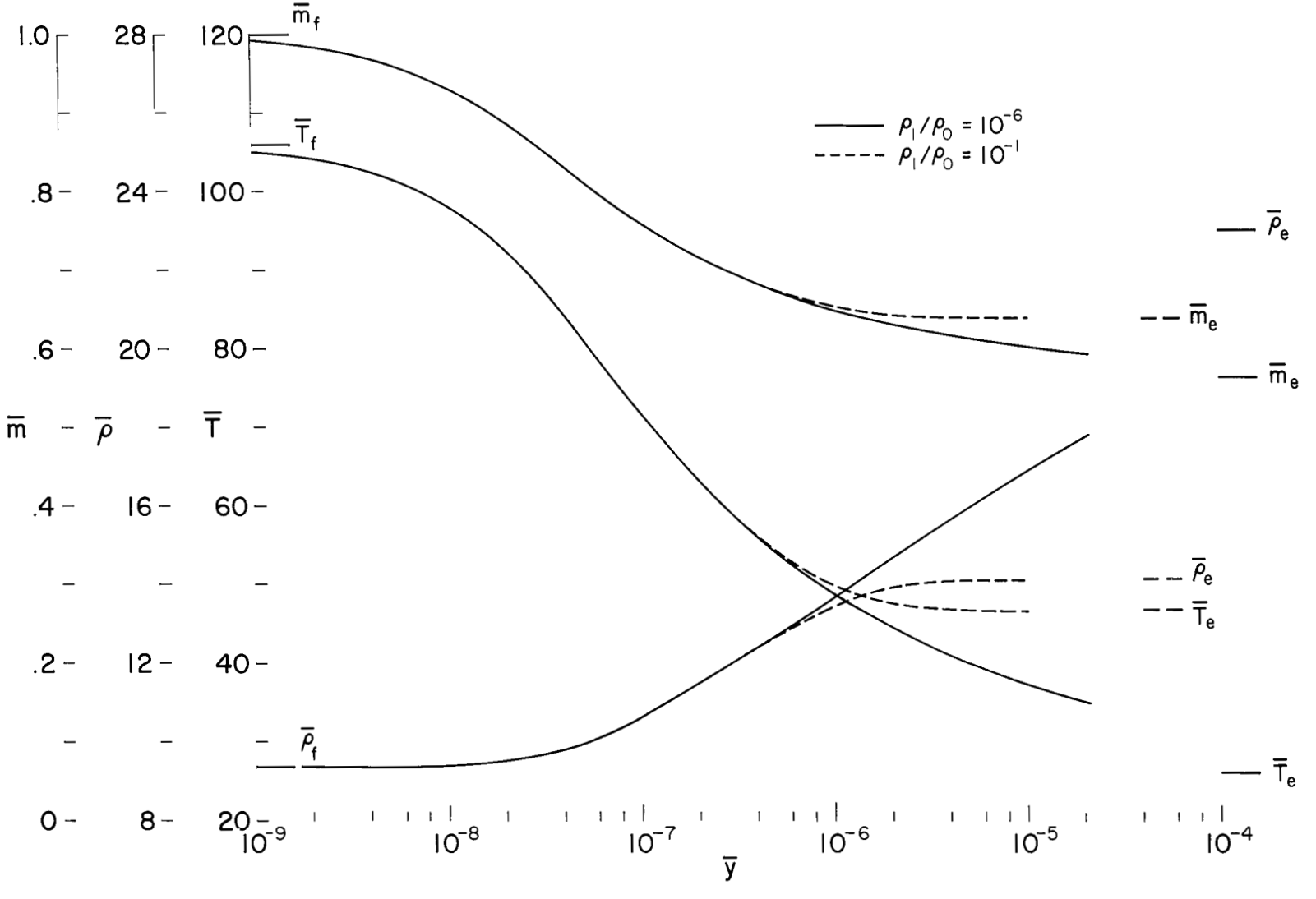

(a) Thermodynamic properties.

Figure 5.- Nonequilibrium profiles; V_s = 8 km/sec in 5 percent CO_2 - 95 percent N_2.

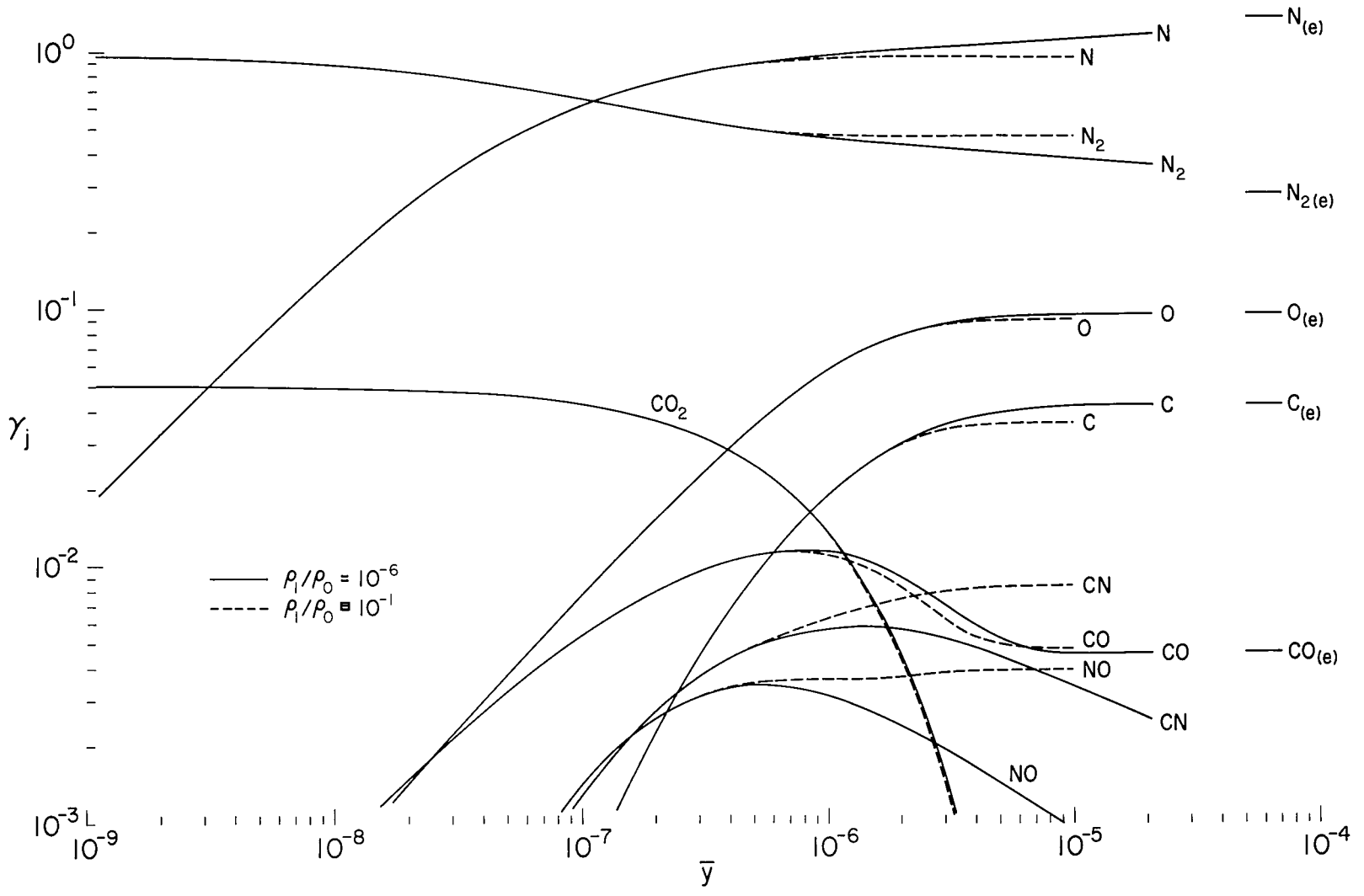

(b) Species concentrations.

Figure 5.- Concluded.

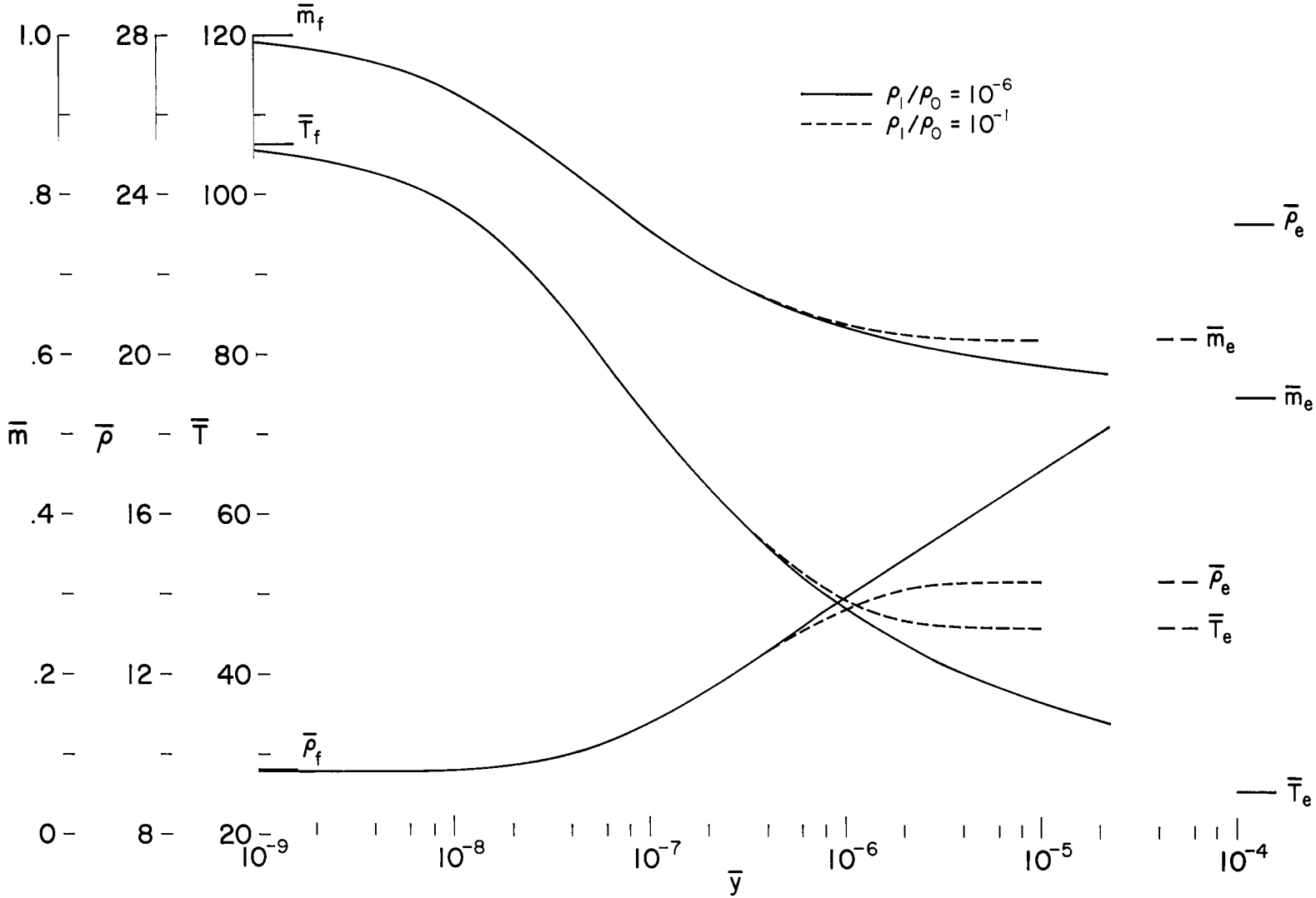

(a) Thermodynamic properties.

Figure 6.- Nonequilibrium profiles; V_s = 8 km/sec in 10 percent CO_2 - 90 percent N_2.

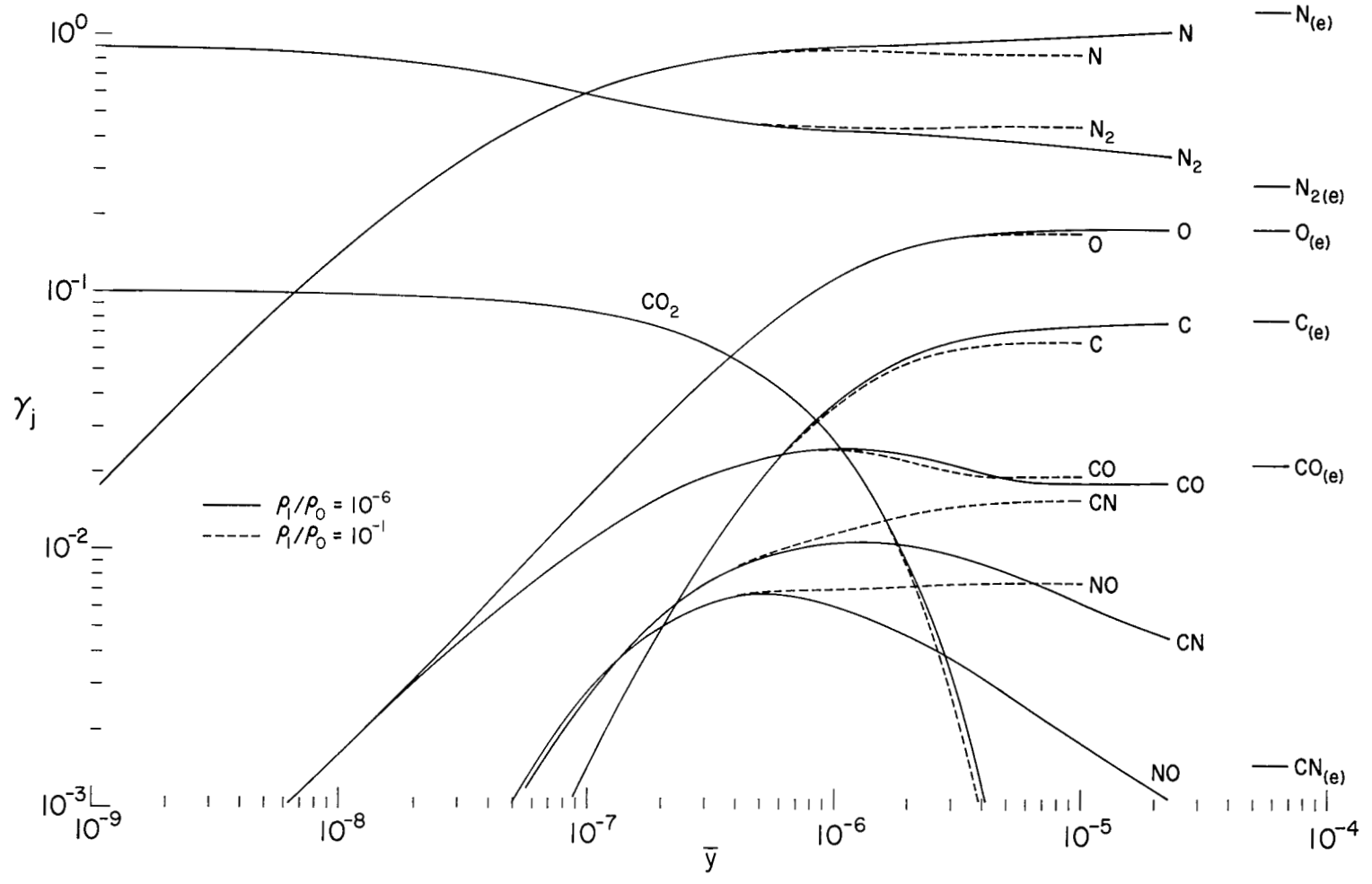

(b) Species concentrations.

Figure 6.- Concluded.

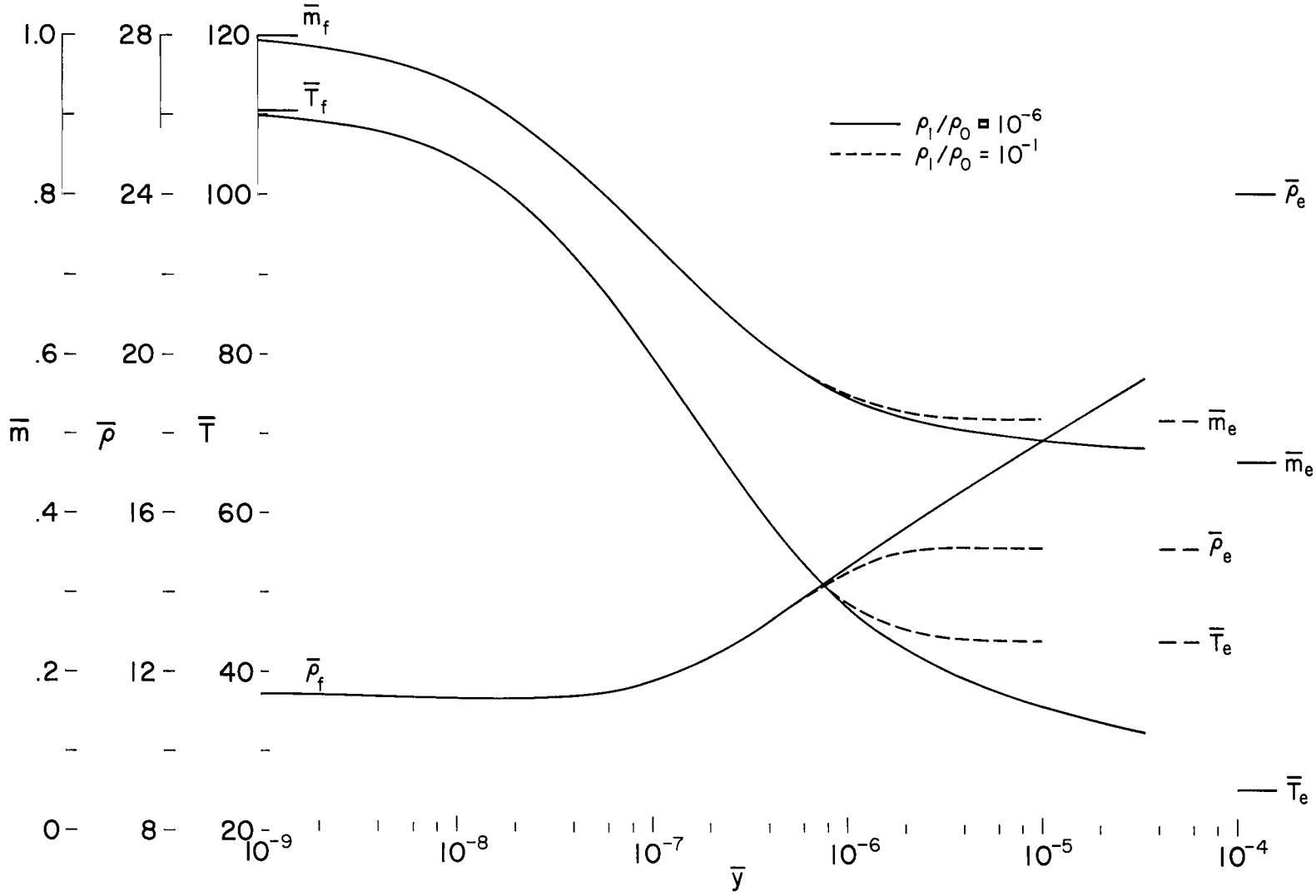

(a) Thermodynamic properties.

Figure 7.- Nonequilibrium profiles; V_S = 8 km/sec in 50 percent CO_2 - 50 percent N_2.

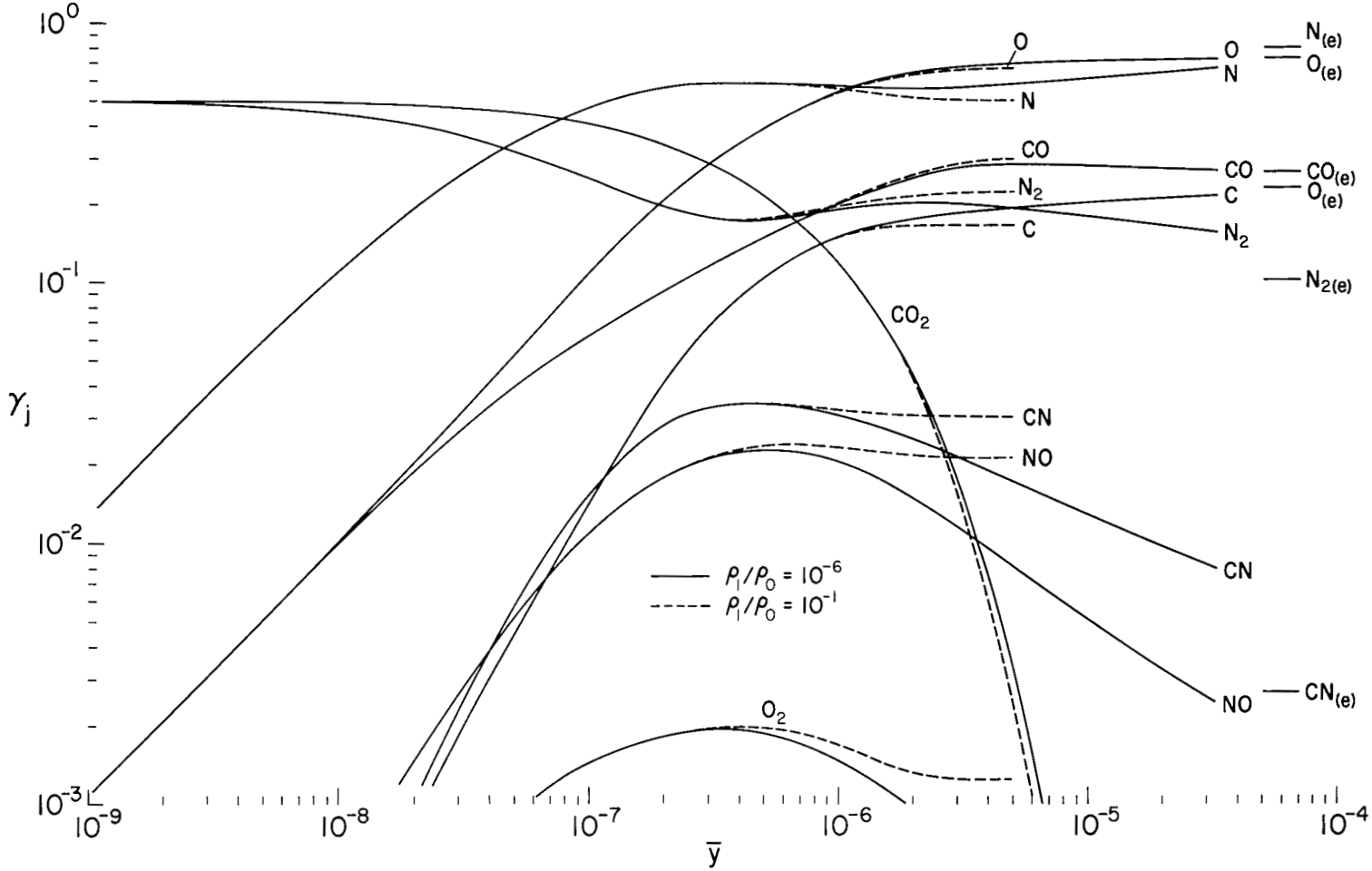

(b) Species concentrations.

Figure 7.- Concluded.

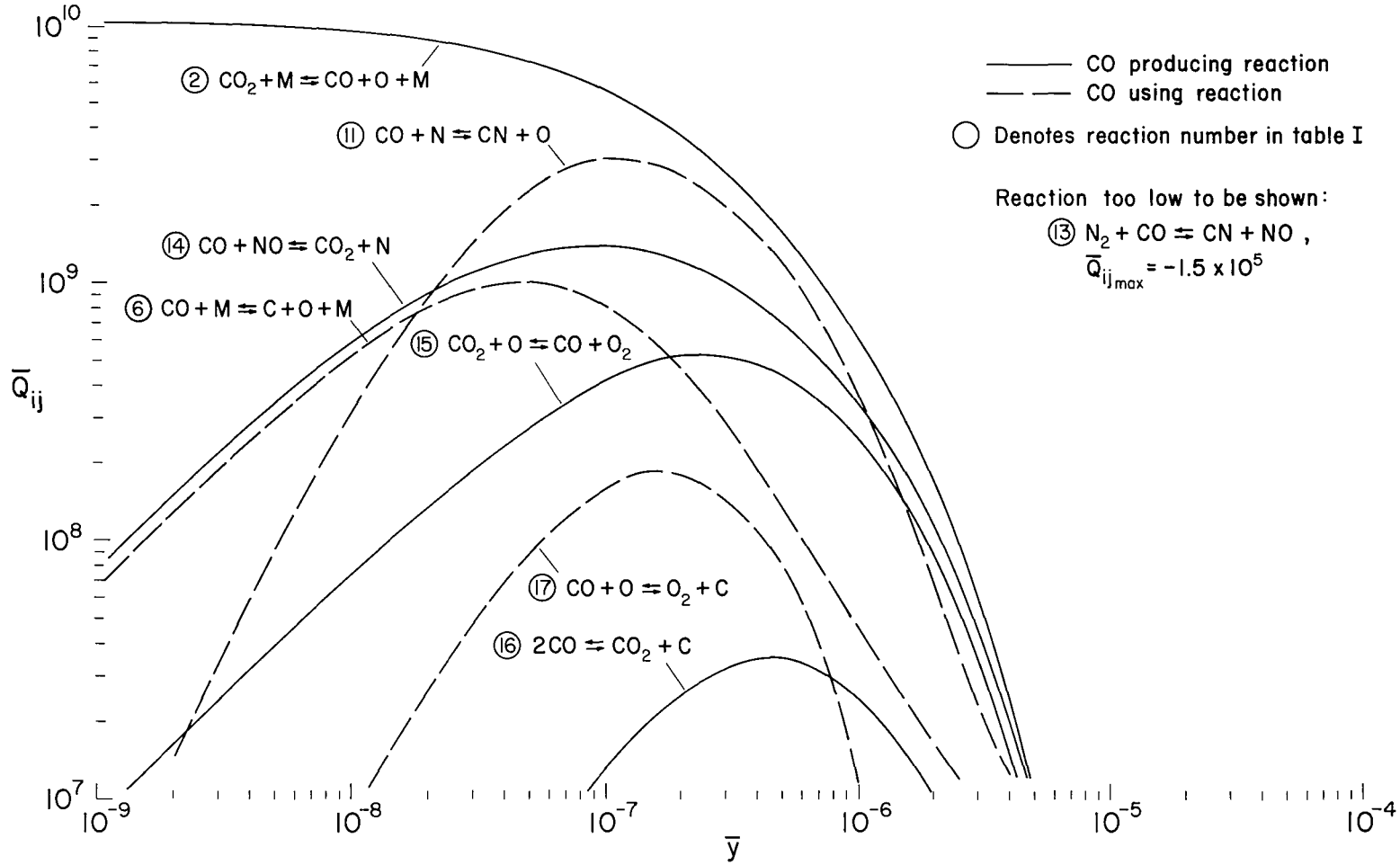

(a) CO production.

Figure 8.- Species production rates for individual reactions; V_s = 8 km/sec in 50 percent CO_2 - 50 percent N_2, $\rho_1/\rho_0 = 10^{-6}$.

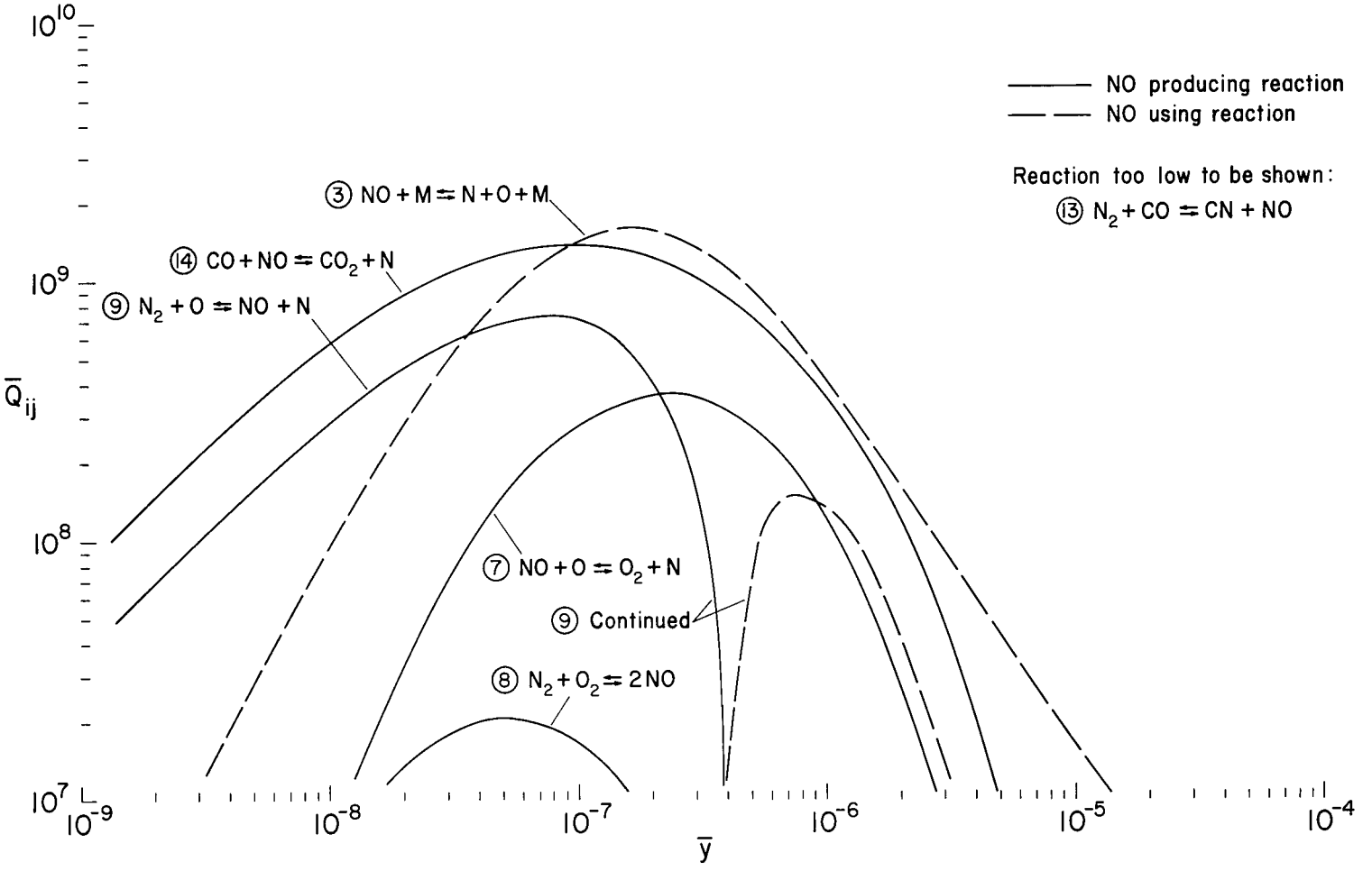

(b) NO production.

Figure 8.- Continued.

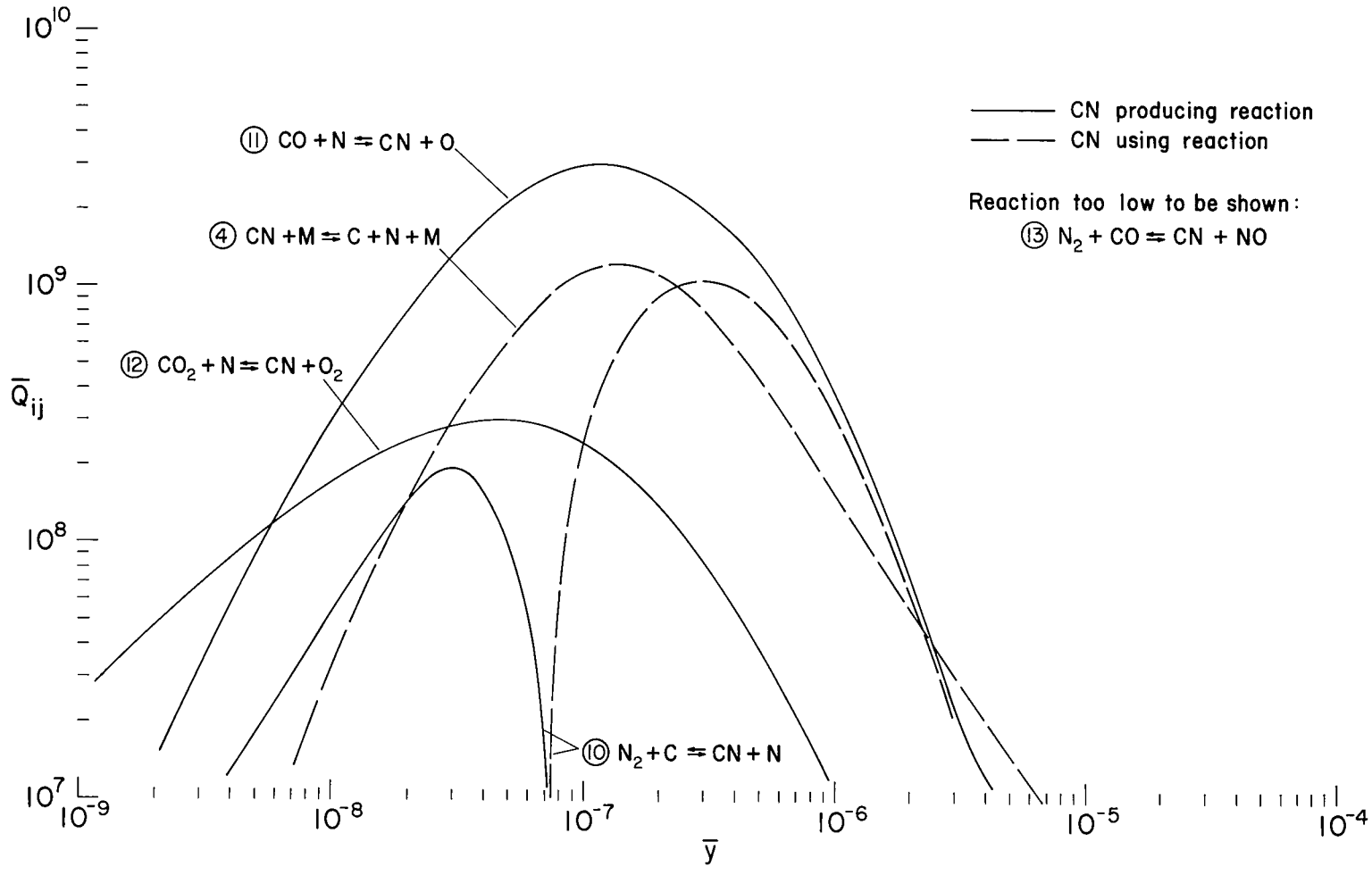

(c) CN production.

Figure 8.- Continued.

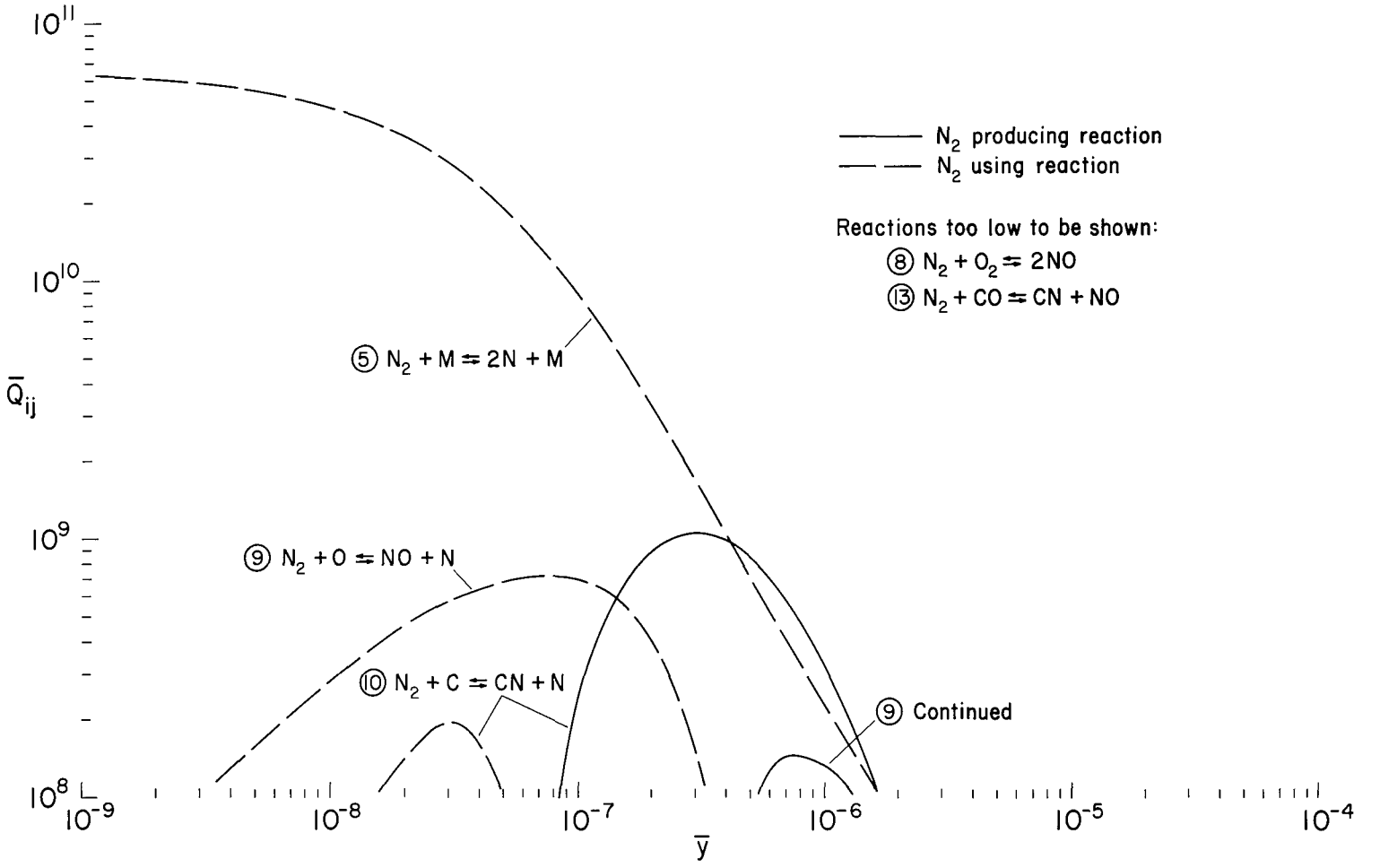

(d) N_2 production.

Figure 8.- Continued.

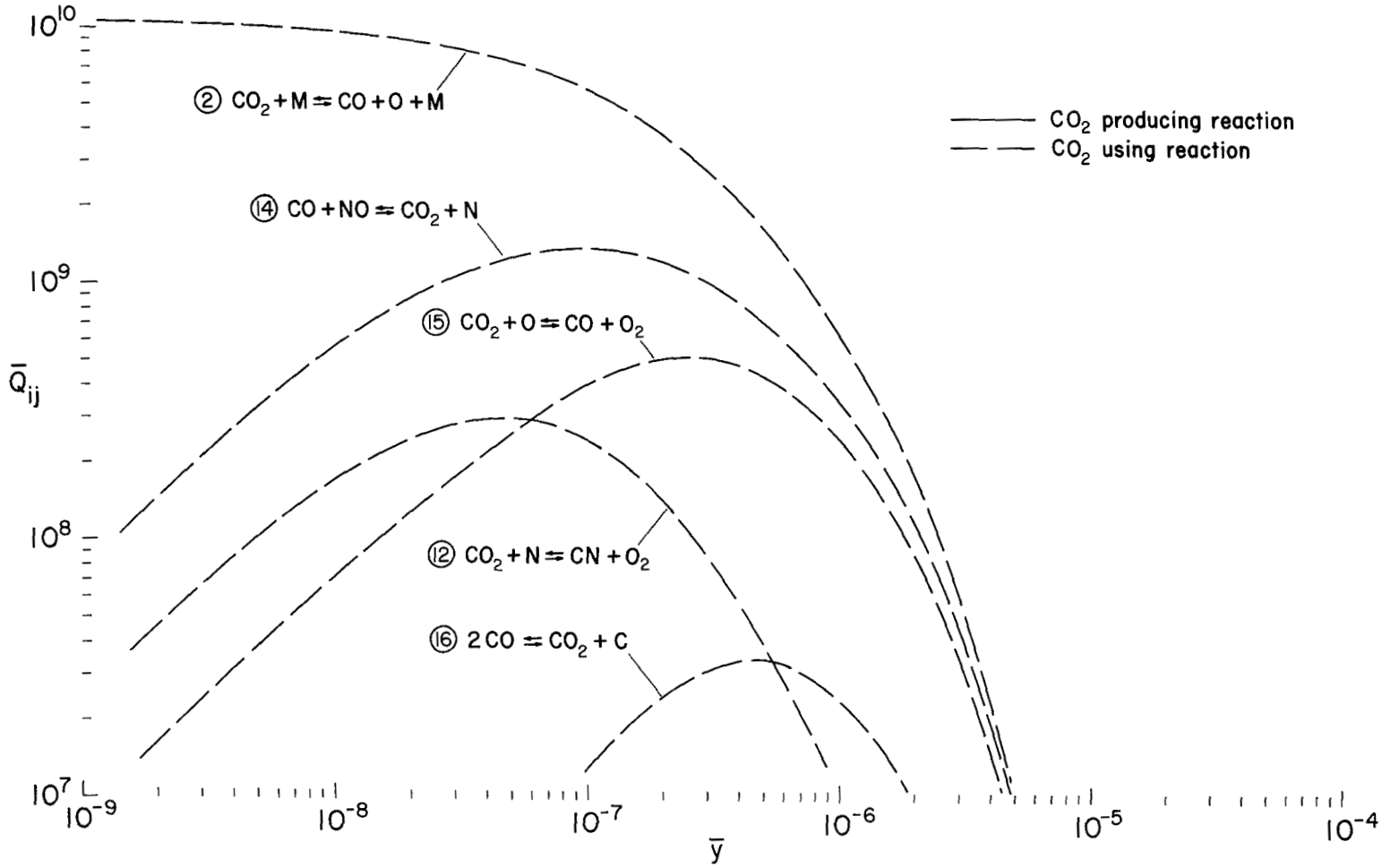

(e) CO_2 production.

Figure 8.- Continued.

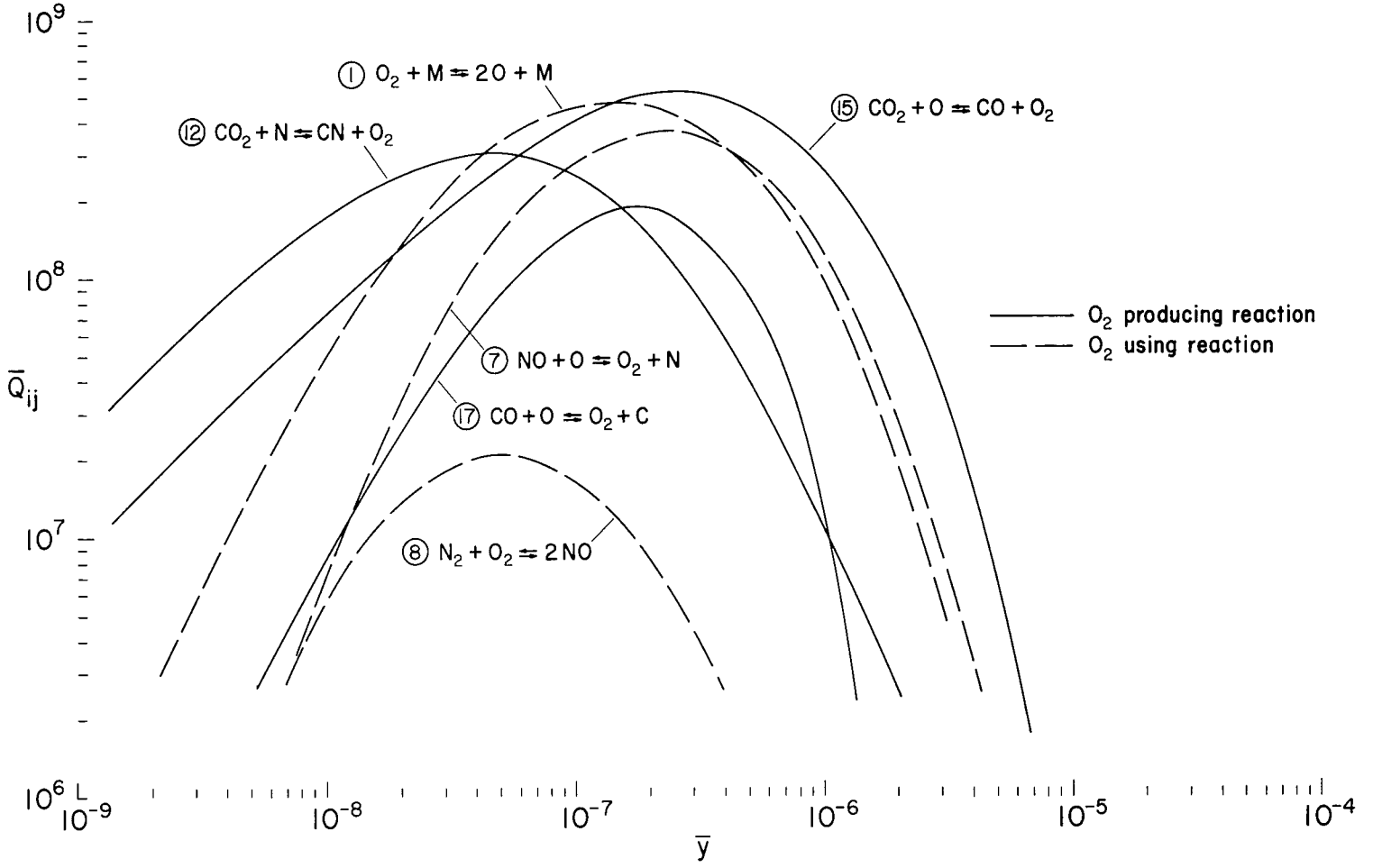

(f) O_2 production.

Figure 8.- Concluded.

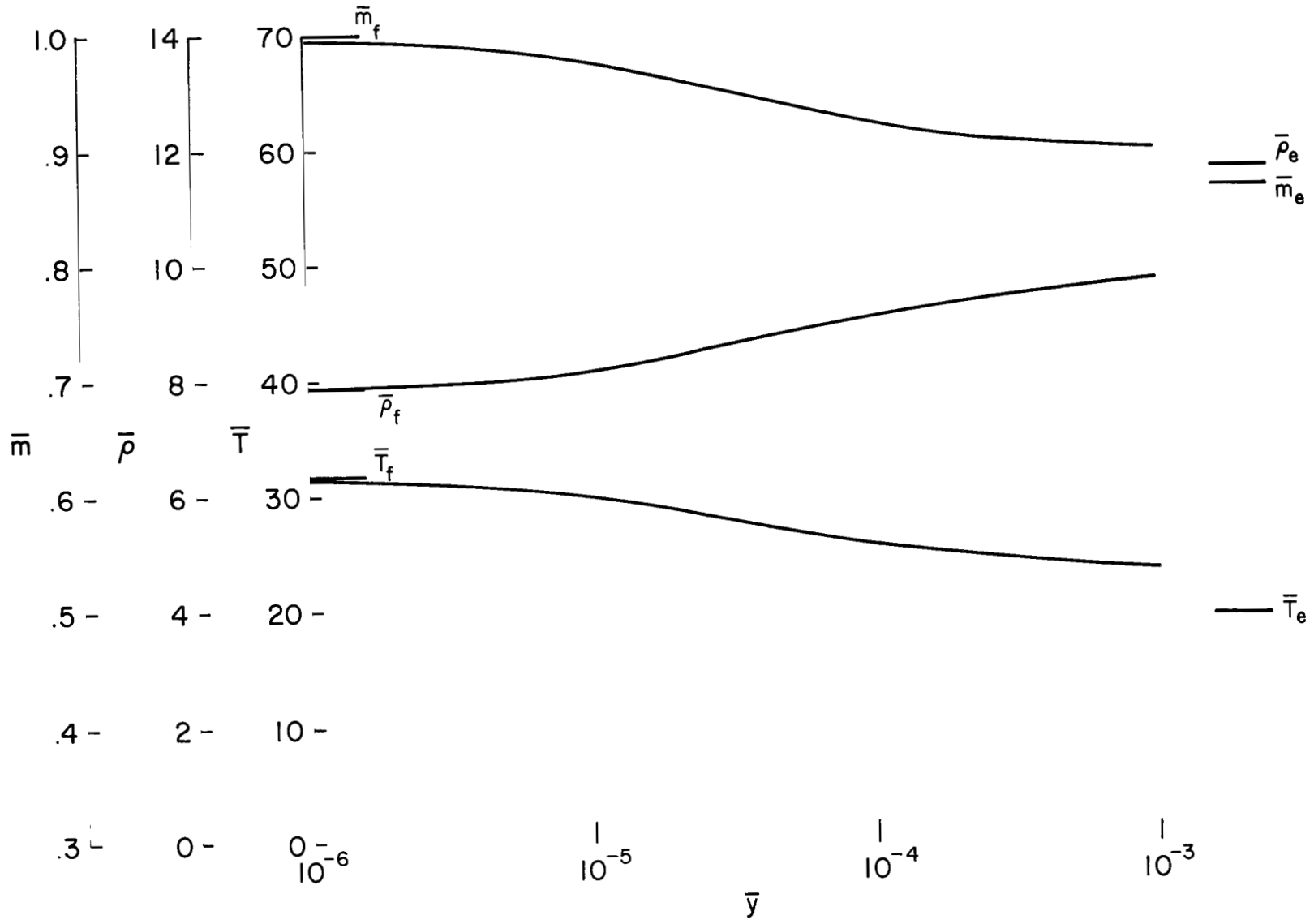

(a) Thermodynamic properties.

Figure 10.- Nonequilibrium profiles; V_s = 4 km/sec in 10 percent CO_2 - 90 percent N_2, $\rho_1/\rho_0 = 10^{-6}$.

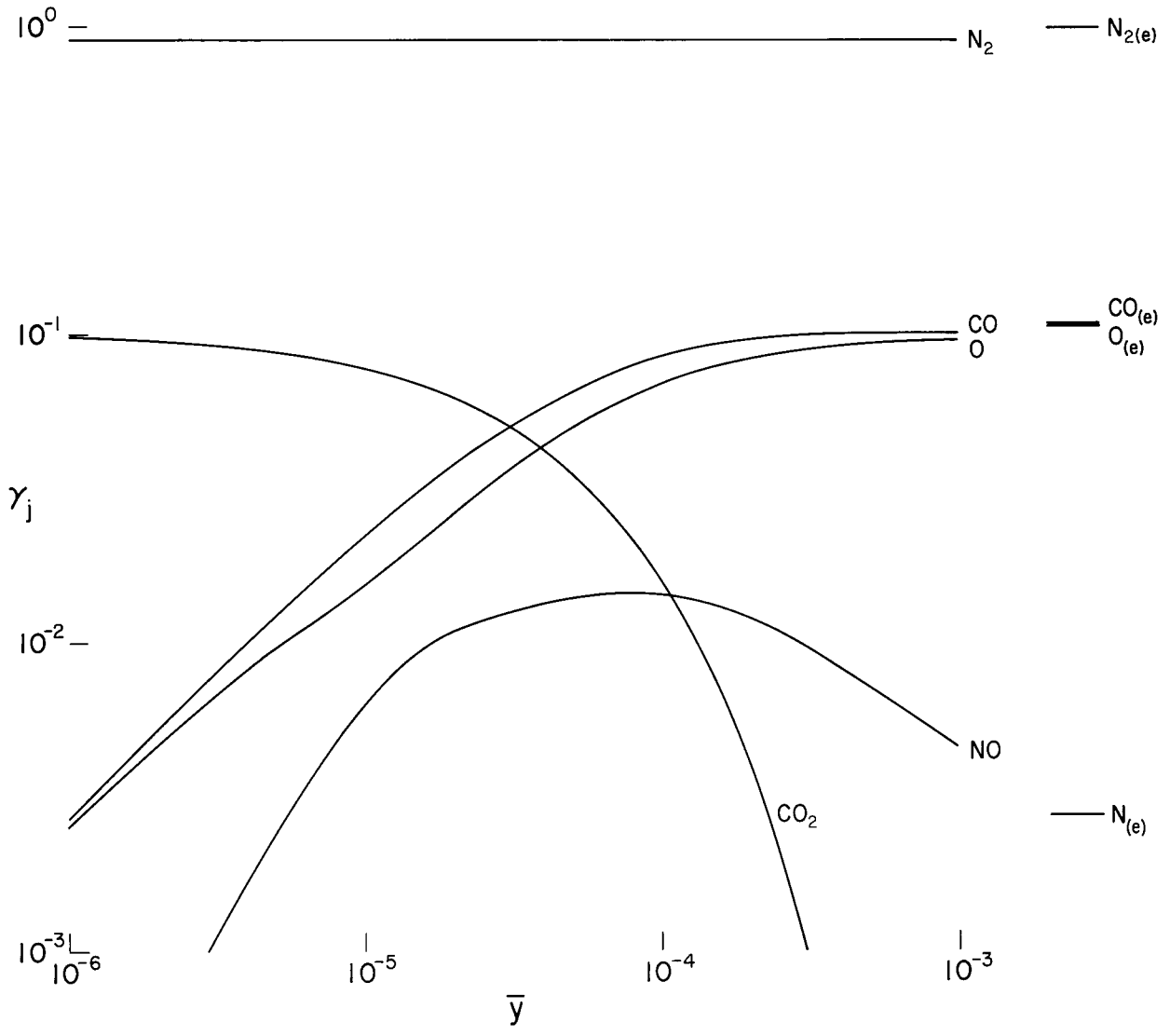

(b) Species concentrations.

Figure 10.- Concluded.

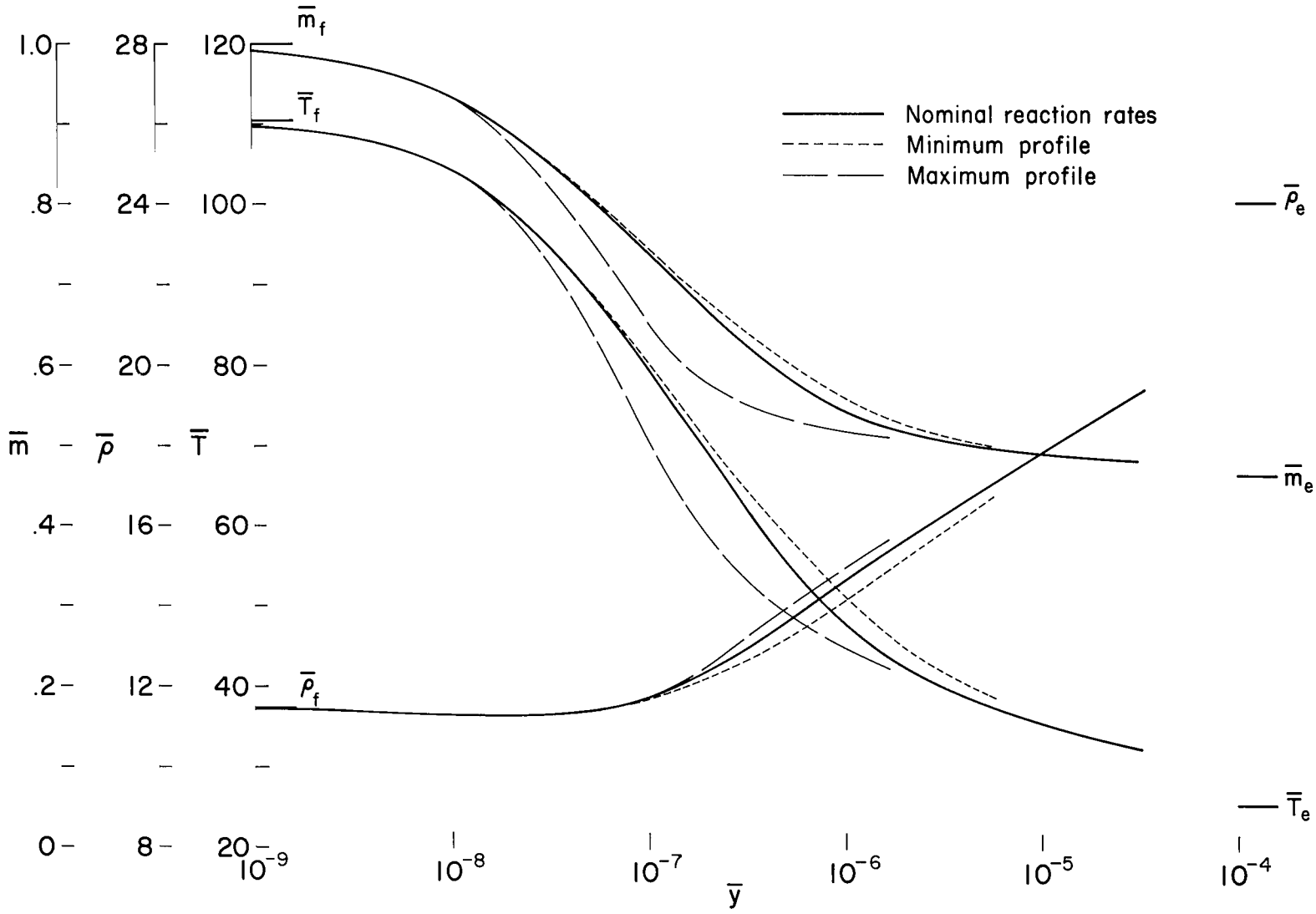

(a) Thermodynamic properties.

Figure 11.- The effects of uncertain reaction rates; V_S = 8 km/sec in 50 percent CO_2 - 50 percent N_2, $\rho_1/\rho_o = 10^{-6}$.

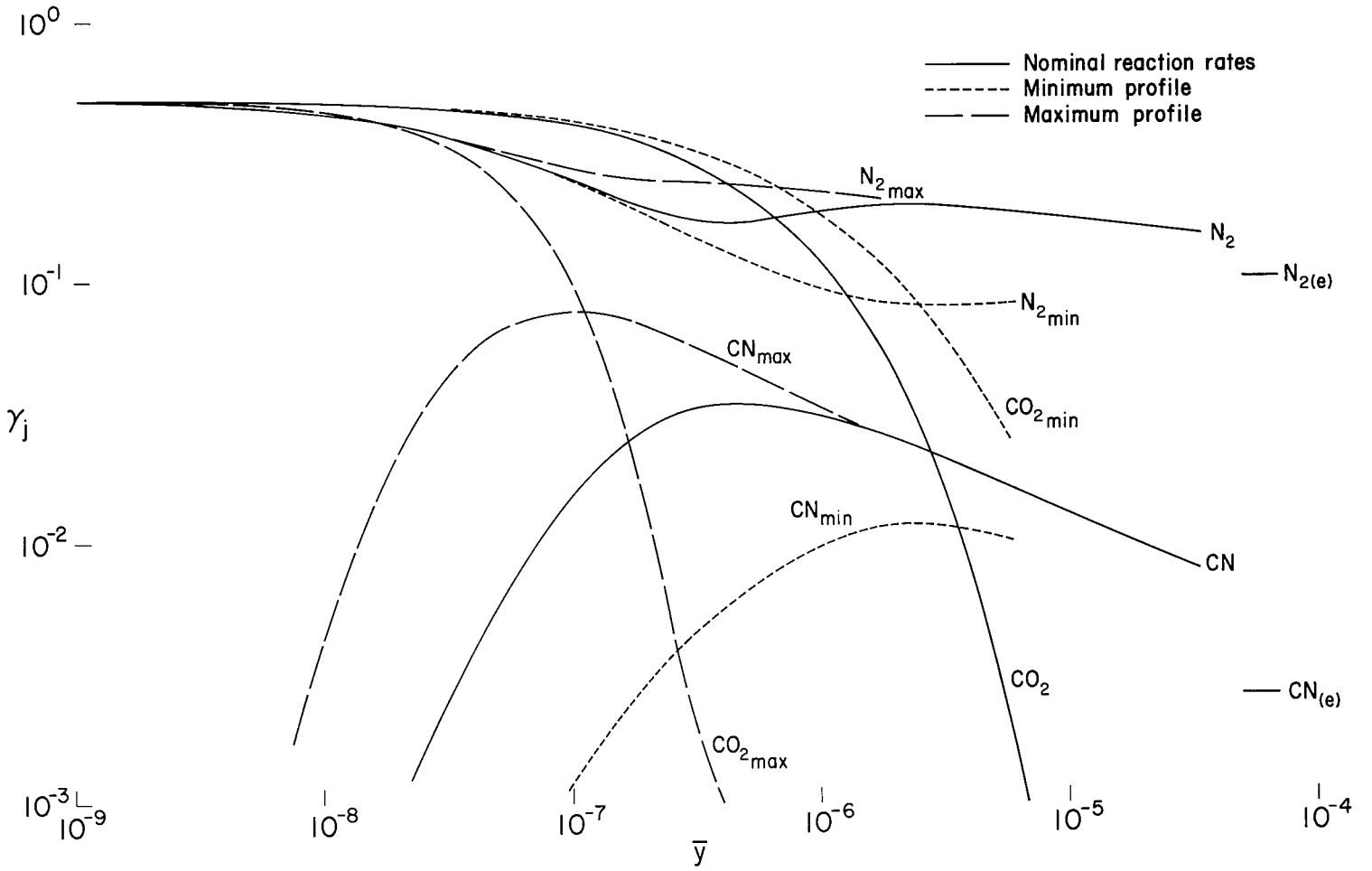

(b) CN, N_2, and CO_2 concentrations.

Figure 11.- Continued.

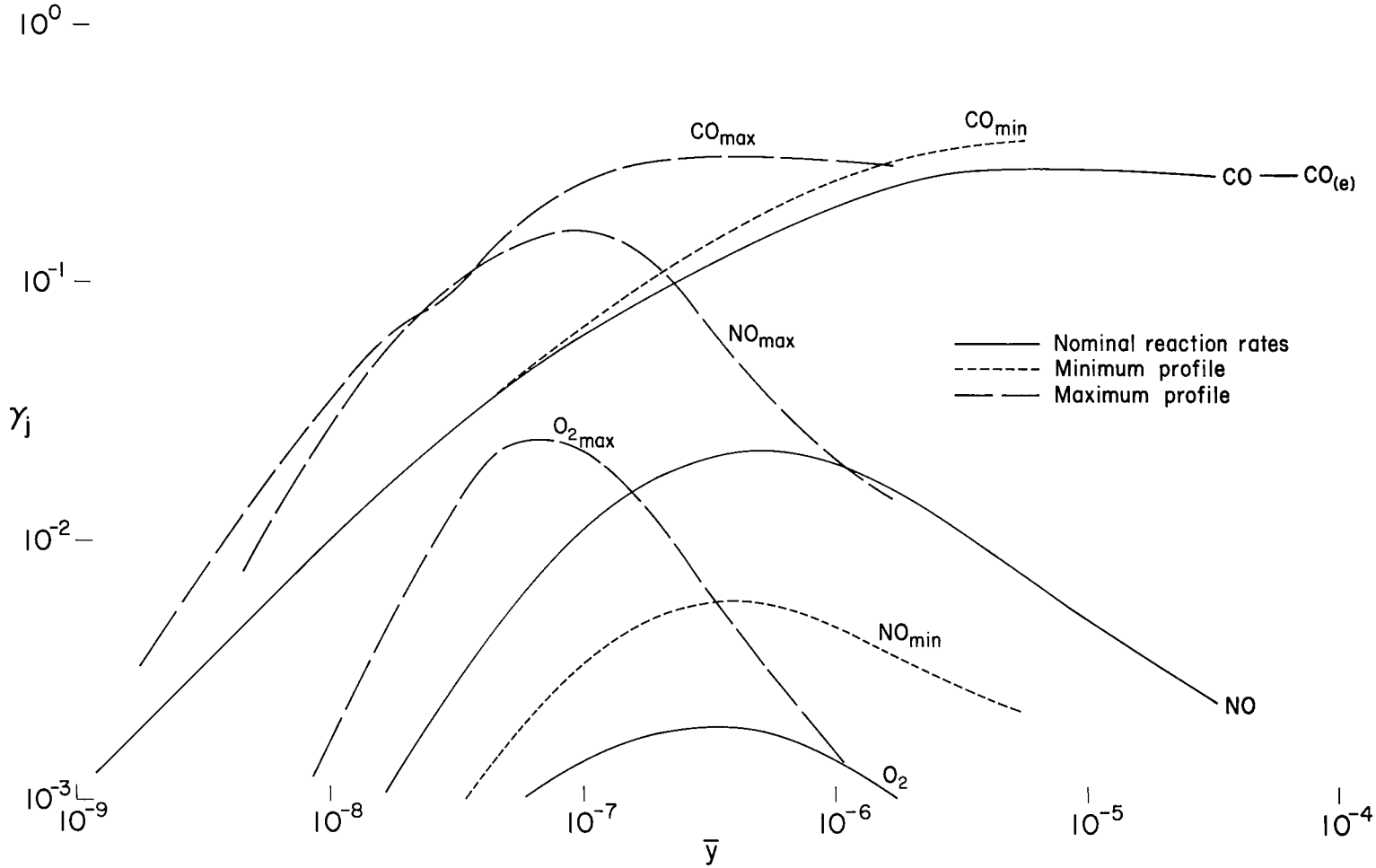

(c) CO, NO, and O_2 concentrations.

Figure 11.- Concluded.

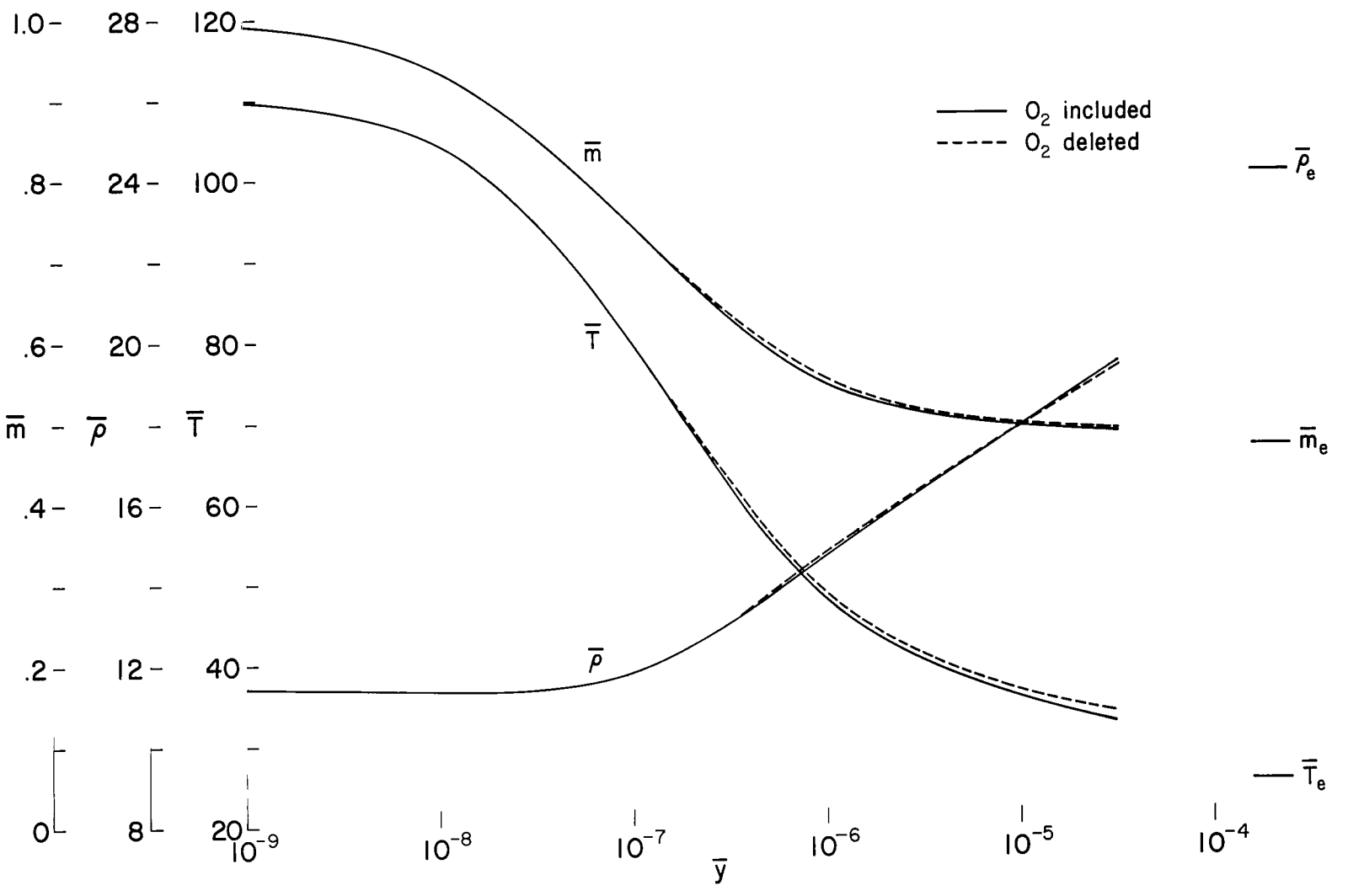

(a) Thermodynamic properties.

Figure 12.- The effect of deleting O_2 reactions; V_S = 8 km/sec in 50 percent CO_2 - 50 percent N_2, $\rho_1/\rho_0 = 10^{-6}$.

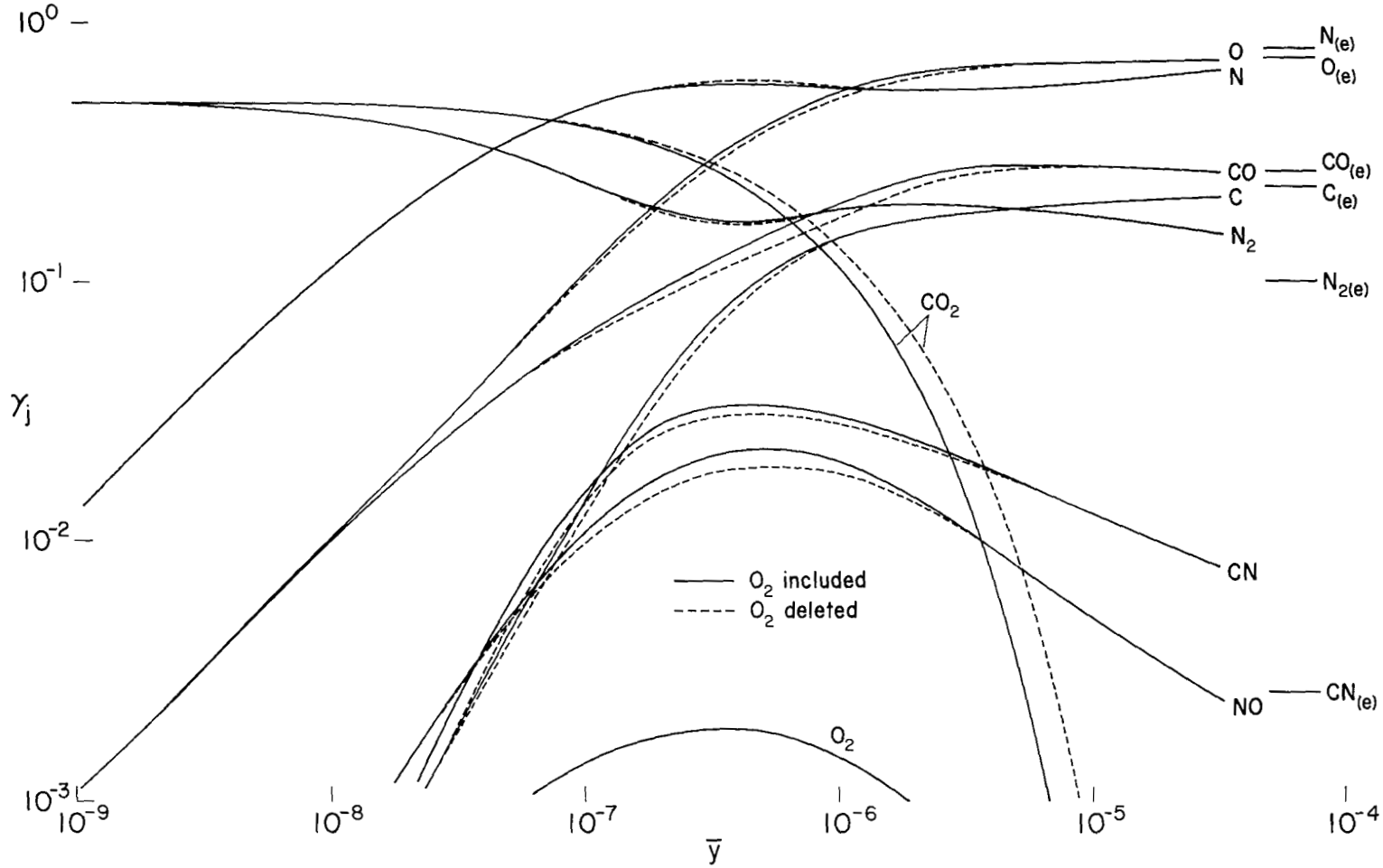

(b) Species concentrations.

Figure 12.- Concluded.

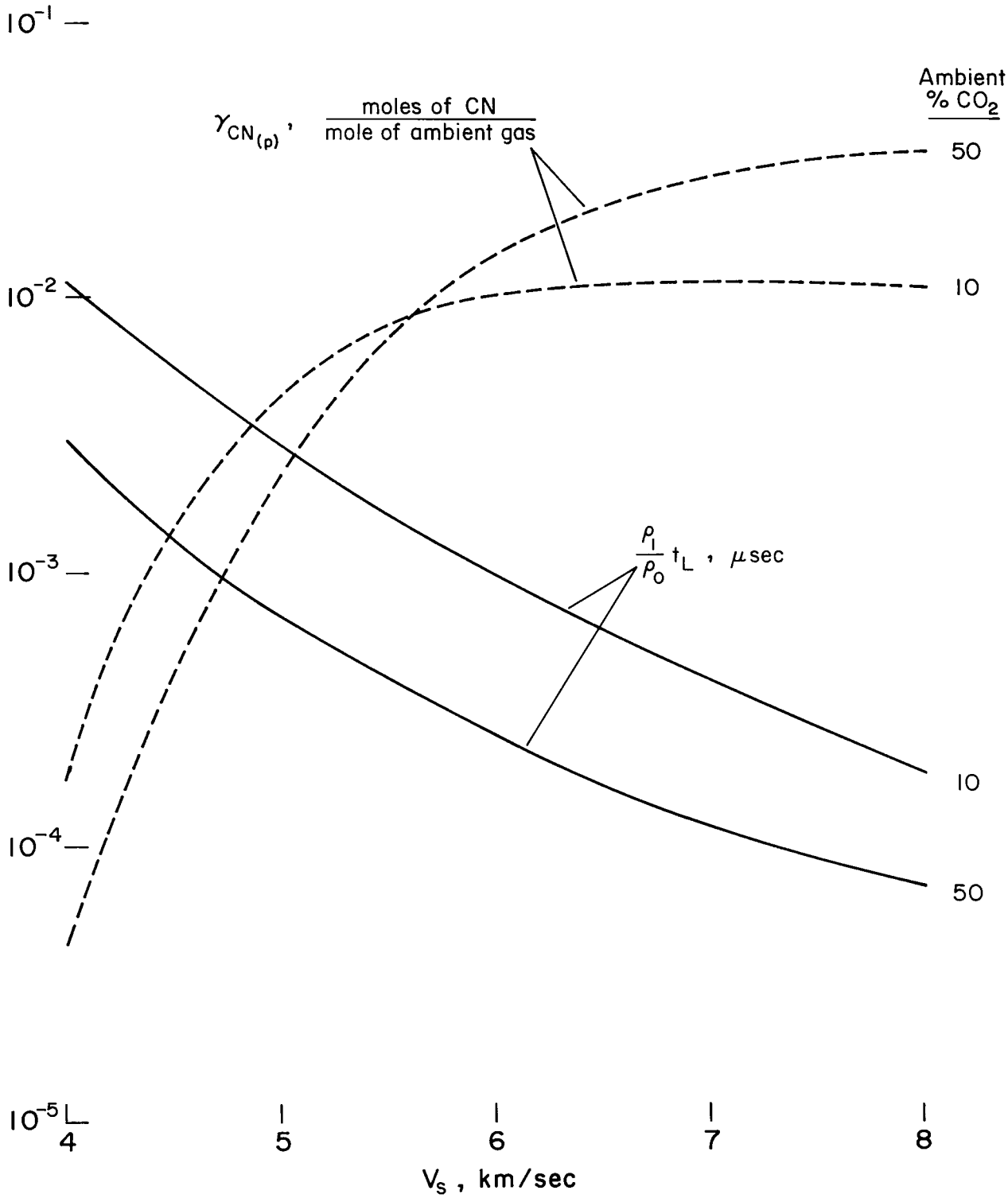

Figure 13.- Laboratory time and magnitude of the peak CN concentration using nominal reaction rates.

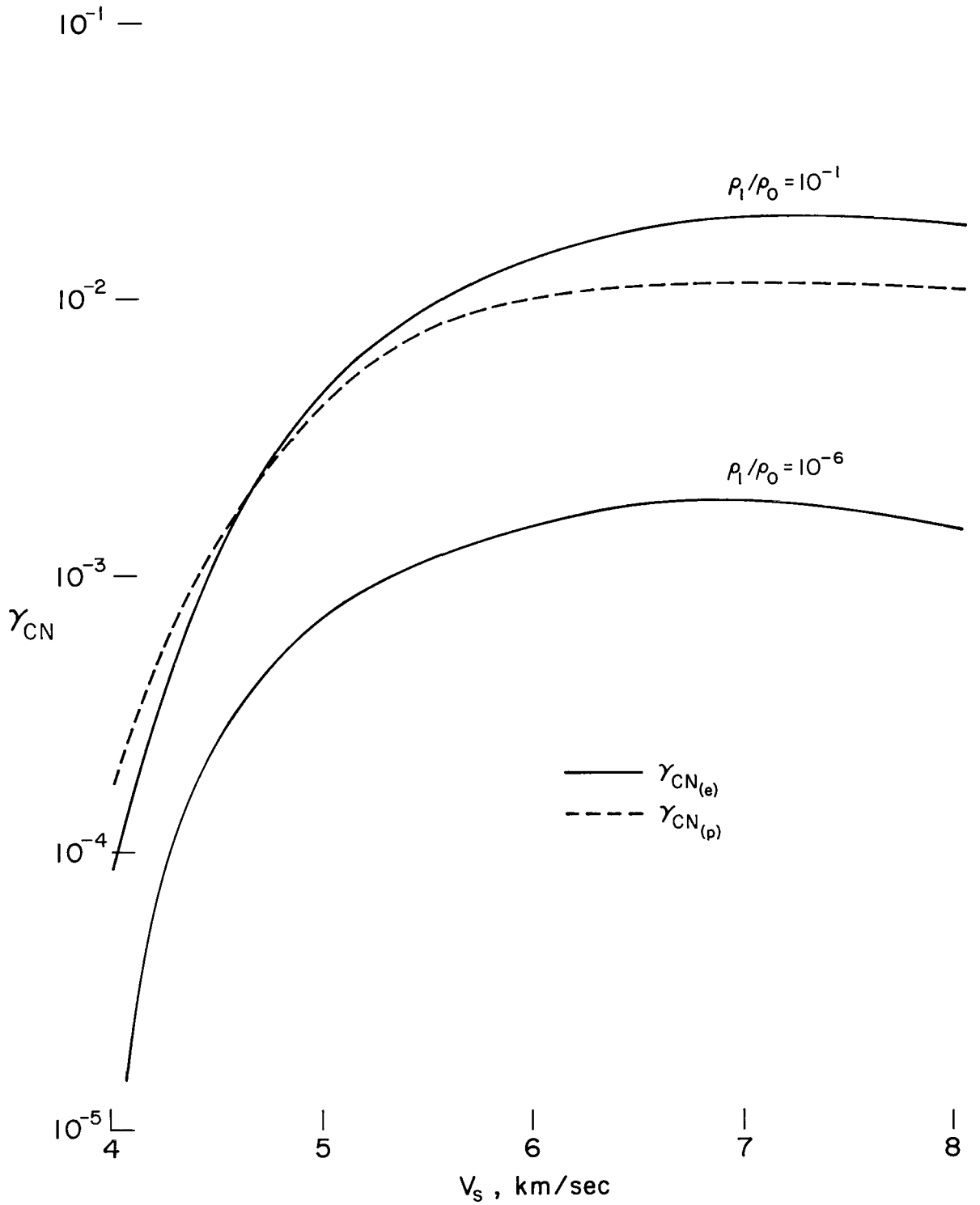

(a) 10 percent CO_2 - 90 percent N_2.

Figure 14.- Peak and equilibrium CN concentrations.

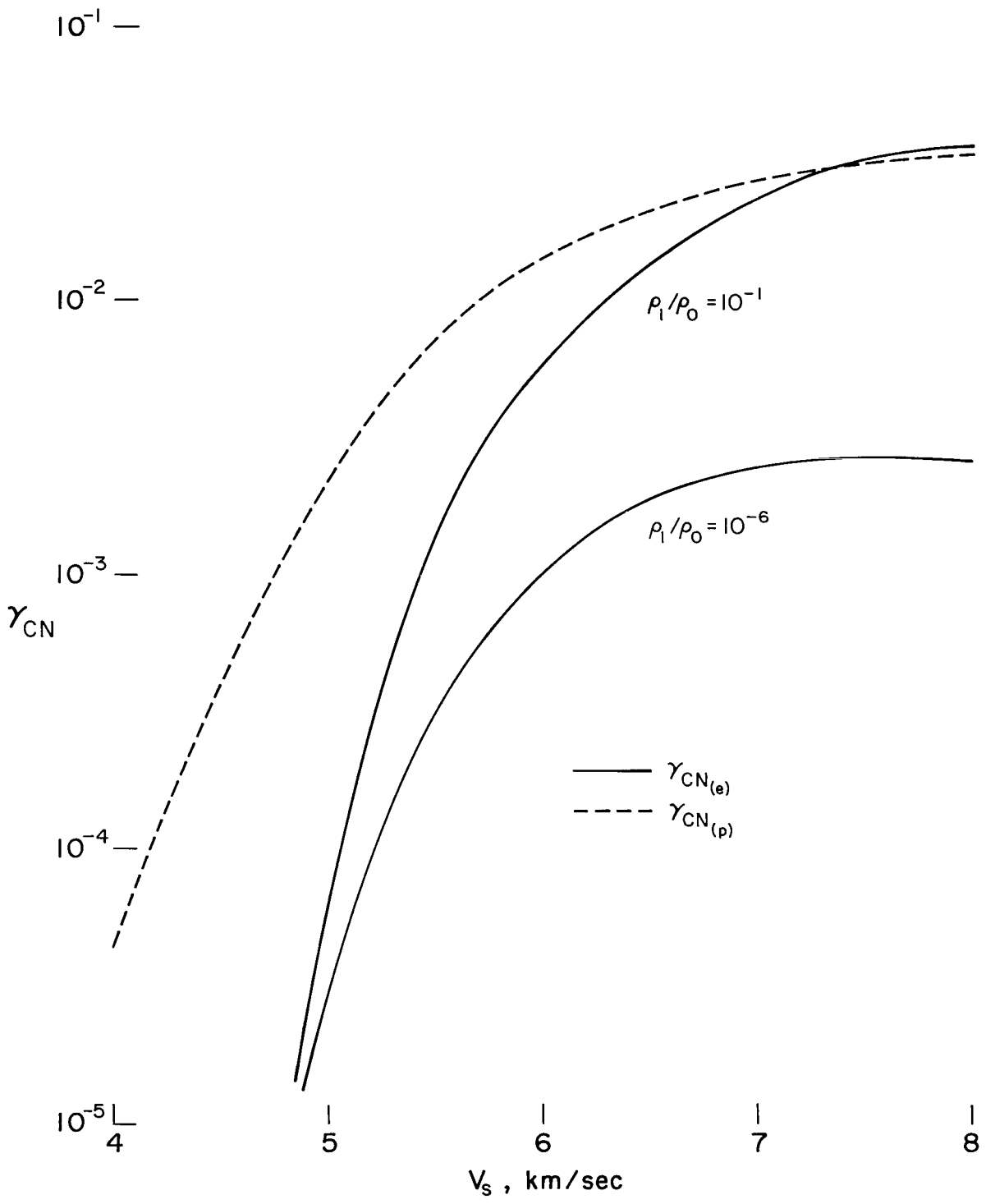

(b) 50 percent CO_2 - 50 percent N_2.

Figure 14.- Concluded.

"The aeronautical and space activities of the United States shall be conducted so as to contribute . . . to the expansion of human knowledge of phenomena in the atmosphere and space. The Administration shall provide for the widest practicable and appropriate dissemination of information concerning its activities and the results thereof."

—NATIONAL AERONAUTICS AND SPACE ACT OF 1958

NASA SCIENTIFIC AND TECHNICAL PUBLICATIONS

TECHNICAL REPORTS: Scientific and technical information considered important, complete, and a lasting contribution to existing knowledge.

TECHNICAL NOTES: Information less broad in scope but nevertheless of importance as a contribution to existing knowledge.

TECHNICAL MEMORANDUMS: Information receiving limited distribution because of preliminary data, security classification, or other reasons.

CONTRACTOR REPORTS: Technical information generated in connection with a NASA contract or grant and released under NASA auspices.

TECHNICAL TRANSLATIONS: Information published in a foreign language considered to merit NASA distribution in English.

TECHNICAL REPRINTS: Information derived from NASA activities and initially published in the form of journal articles.

SPECIAL PUBLICATIONS: Information derived from or of value to NASA activities but not necessarily reporting the results of individual NASA-programmed scientific efforts. Publications include conference proceedings, monographs, data compilations, handbooks, sourcebooks, and special bibliographies.

Details on the availability of these publications may be obtained from:

SCIENTIFIC AND TECHNICAL INFORMATION DIVISION

NATIONAL AERONAUTICS AND SPACE ADMINISTRATION

Washington, D.C. 20546